Journal of Achievements in Materials and Manufacturing Engineering
VOLUME 47
ISSUE 2
August
2011

Fraction solid evolution characteristics of AlSiCu alloys - dynamic baseline approach

P. Marchwica, J.H. Sokolowski*, W.T. Kierkus
Department of Mechanical, Automotive and Materials Engineering,
University of Windsor, 401 Sunset Avenue, Windsor,
Ontario, N9B 3P4, Canada
* Corresponding author: E-mail address: jerry@uwindsor.ca

Received 17.06.2011; published in revised form 01.08.2011

Materials

ABSTRACT

Purpose: The goal of the research presented in this paper is to gain a deeper understanding of dynamic solidification processes of metals and alloys through application of improved baseline and fraction solid methodologies to hypoeutectic aluminum-silicon alloys with varying concentrations of silicon and copper.
Design/methodology/approach: The paper makes use of numerical models developed at the University of Windsor, including Newtonian Computer-Aided Cooling Curve Analysis and the Silicon Equivalency algorithm. Co-developed thermal analysis platforms are also used, including the Universal Metallurgical Simulator and Analyzer (UMSA) and the Aluminum Thermal Analysis Platform (AlTAP).
Findings: This paper identifies key temperature and fraction solid values for hypoeutectic AlSiCu alloys across a wide range of chemistries. The paper also provides correlations whereby temperature/fraction solid values for metallurgical reactions can be predicted on the basis of chemistry.
Research limitations/implications: Future work for the project will expand upon the relationships between important metallurgical events and alloy chemistries and derive general trends to enhance predictive capabilities.
Practical implications: The data and techniques used in this paper may be used in order to improve simulations of casting processes. The relationships between solidification events and alloy chemistries will aid in the design and optimization of casting alloys and components.
Originality/value: This paper would be of value to members of the engineering community who need precise information about fraction solid for use in designing alloys or optimizing technology and simulations of casting processes.
Keywords: Aluminum alloys; Baseline; Fraction solid; Thermal analysis

Reference to this paper should be given in the following way:
P. Marchwica, J.H. Sokolowski, W.T. Kierkus, Fraction solid evolution characteristics of AlSiCu alloys - dynamic baseline approach, Journal of Achievements in Materials and Manufacturing Engineering 47/2 (2011) 115-136.

1. Introduction

1.1. Research overview

Advanced Thermal Analysis of a metal or alloy's heating and cooling curve can provide a wide range of vital quantitative metallurgical information. This data includes:

- The effect of the melt's chemical composition, its treatment(s) and solidification environment on latent heat of solidification.
- Fraction solid evolution (including apparent f_s for individual metallurgical reactions).
- Dendrite coherency point characteristics.
- Assessment of riser efficiency.

Cooling curve data can also be used to predict characteristics such as Secondary Dendrite Arm Spacing (SDAS), the Silicon Modification Level (SiML for AlSi cast components) and the level of grain refinement that relates to in-service cast component performance. Heating curve data is an indispensible tool for optimization of the heat treatment processes, and semi-solid casting technology, etc. [1-8].

In order to extract the above-mentioned scientific data it is necessary to first compute the Dynamic Baseline curve (***DBL*** for short) for material tested under specifically selected environmental conditions. This must be completed prior to in-depth thermal analysis of metallurgical characteristics of the heating/cooling curve. A ***DBL*** is determined for the temperature change during the cooling/solidification and heating/melting cycles' varying rates. By definition, a ***DBL*** represents the part of a hypothetical first derivative of the experimental cooling/heating curve that would exist if no phase transformation (metallurgical reaction(s) including melting and solidification events) occurred during the solidification and/or melting process. The ***DBL*** equation accounts for the unique tested material/melt characteristics and its processing conditions in which no latent heat is released or absorbed. It can also be interpreted as a measure of the "scaled" rate of energy loss from the test sample under particular test conditions. Therefore, the ***DBL*** function represents both simple and complex processed material/cast component characteristics and industrial conditions that UMSA can precisely simulate. Unfortunately, in their seminal work on cooling curve analysis, Bäckerud et al. [9] did not present a procedure for ***DBL*** equation calculation.

Fraction solid (f_s) may be defined as the percentage of solid phase(s) formed between the equilibrium and/or non-equilibrium liquidus and solidus temperatures in a solidifying melt of metal, alloy and metal matrix composite. f_s can be expressed numerically as a value in the range [0, 1] or as a percentage. Fraction Liquid (f_L), often used for the assessment of semi-solid processing parameters, can be defined as $\mathbf{1 - f_s}$

Successful designing of an alloy system, cast component and its manufacturing technology as well as execution of on-line metallurgical process control requires quantitative knowledge about solidification events such as f_s evolution which directly affects the as-cast structure. More specifically, most cast components contain different cross sectional thicknesses or use specific geometries (i.e. fins, chills, etc.) that result in different solidification rates. These rates influence some cooling curve characteristics including f_s evolution parameters which in turn affect feeding modes and determine the as-cast structure (i.e. phase type, its morphology, integrity, etc). In turn, the as-cast structure directly dictates further technological processes including heat treatment operations for the optimized in-service cast component performance.

This paper provides details about the University of Windsor methodology for f_s analysis utilized in its technology platforms, namely the AlTAP and the UMSA - co-developed with Dr. Marcin Kasprzak of Silesian University of Technology in Poland [10]. This paper provides examples of AlTAP's and UMSA's f_s characteristics for metals and complex industrial alloys.

Selected information about other techniques for determination of the f_s data is presented in the Literature Review section. The sheer variety of theoretical and empirical methodologies present in the literature for determination of $f_s = f(T \& t)$ characteristics is the best indicator of their paramount importance to the metallurgical science and applied engineering fields. This importance is critical for optimization of cast, wrought and welded metal products and their technologies.

1.2. Selected thermal characteristics of metallurgical reactions

Thermal Analysis - The study of material properties and cast component thermal characteristics as they change with temperature. Though this paper refers to thermal analysis as the process of measuring the temperature changes in a metallic sample via a thermocouple during a heating/cooling cycle, many forms of thermal analysis exist, including differential scanning calorimetry and dilatometry.

Cooling Curve - The portion of the measured temperature vs. time plot that depicts a sample's decrease in temperature after heating is completed. The cooling curve usually covers at least the range where a sample goes from fully liquid to fully solid (also known as the 'semi-solid region' or 'mushy zone').

First Derivative - Refers to the first derivative of the cooling curve (dT_c/dt) and is used because it makes metallurgical events more visually prominent.

Cooling Curve Analysis - Extracting metallurgical information based on analysis of cooling curves, as well as derivatives, baselines, fraction solids, etc. Most analysis is now in the form of Computer Aided Cooling Curve Analysis (**CA-CCA**).

Undercooling - The event when a solidifying sample's temperature goes below its transformation temperature without experiencing a phase transformation. The degree of undercooling (difference between the highest and lowest temperatures recorded during the event) is affected by several factors, including solidification rate and inclusions. An example of undercooling is seen in Figure 1 at approx. 150 s.

Recalescence - The ending portion of an undercooling event where the sample's temperature rises and returns to its transformation temperature.

Cooling/Solidification Rate - Though sometimes used interchangeably, the solidification rate refers to the rate of temperature decrease in a sample during phase transformations, while the cooling rate is used only during fully liquid/fully solid temperature changes.

Baseline - The theoretical path that the first derivative of the temperature curve would follow if no metallurgical transformations were to occur. Though a baseline can be calculated using both heating and cooling processes, only those calculated during cooling are used throughout this paper (unless otherwise indicated).

Dynamic Baseline - There are several methods in the literature for determining a baseline path. The Dynamic Baseline (referred to as the ***DBL*** in this paper) refers to the specific methodology for choosing a baseline as developed at the University of Windsor and outlined in this paper.

Fraction Solid - A percentage measure of how much of a sample is solid within the semi-solid region, denoted ***fs*** within this paper. It is 0% at the liquidus temperature and 100% at the solidus temperature.

Silicon Equivalency (Si_{EQ}) - A means of equating quantities of alloying and impurity elements in aluminum to an equivalent amount of alloying silicon, based on the effect they have on the melting temperature.

Table 1 contains a summary of metallurgical events that are investigated for alloys in this paper as well as associated abbreviations used.

Table 1.
Summary of detected metallurgical events during solidification of AlSiCu alloys and associated abbreviations

#	Temp Symbol	Fraction Solid Symbol	Meaning
1	T_{liq} / $T^{\alpha,DEN}{}_{NUC}$	0%	The temperature of α Al dendrite nucleation. Identical to liquidus temperature since it is the first solidification transformation.
2	$T^{\alpha,DEN}{}_{MIN}$	$f_s{}^{\alpha,DEN}{}_{MIN}$	α Al undercooling temperature (minimum temperature reached below transformation temperature)
3	$T^{\alpha,DEN}{}_{G}$	$f_s{}^{\alpha,DEN}{}_{G}$	α Al growth temperature (maximum reached above transformation temperature)
4	$T^{\alpha,DEN}{}_{UNDER}$	$f_s{}^{\alpha,DEN}{}_{UNDER}$	Undercooling (Equal to #3 - #2)
5	$T^{AlSi}{}_{E\ NUC}$	$f_s{}^{AlSi}{}_{E\ NUC}$	AlSi eutectic nucleation temperature
6	$T^{AlSi}{}_{E\ MIN}$	$f_s{}^{AlSi}{}_{E\ MIN}$	AlSi eutectic undercooling temperature
7	$T^{AlSi}{}_{E\ G}$	$f_s{}^{AlSi}{}_{E\ G}$	AlSi eutectic minimum temperature
8	$T^{AlSi}{}_{UNDER}$	$f_s{}^{AlSi}{}_{UNDER}$	Undercooling (Equal to #7 - #6)
9	$T^{MgSi}{}_{NUC}$	$f_s{}^{MgSi}{}_{NUC}$	Magnesium silicides (not investigated in this paper)
10	$T^{AlSiCuMg}$	$f_s{}^{AlSiCuMg}$	Copper/Magnesium rich phase nucleation
11	T_{sol}	100%	Solidus temperature

Figures 1-3 contain graphs of some curves used in thermal analysis, namely the cooling curve, the first derivative and the fraction solid curve. The figures also indicate the locations of metallurgical events outlined in Table 1.

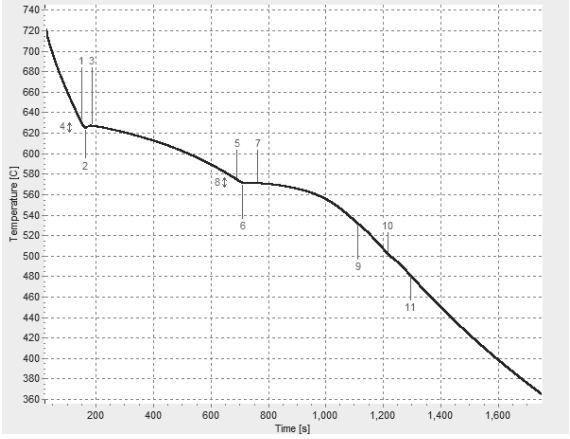

Fig. 1. Temperature vs. Time Cooling Curve of a Nominal 5 wt.% Si and 1 wt.% Cu Aluminum Alloy

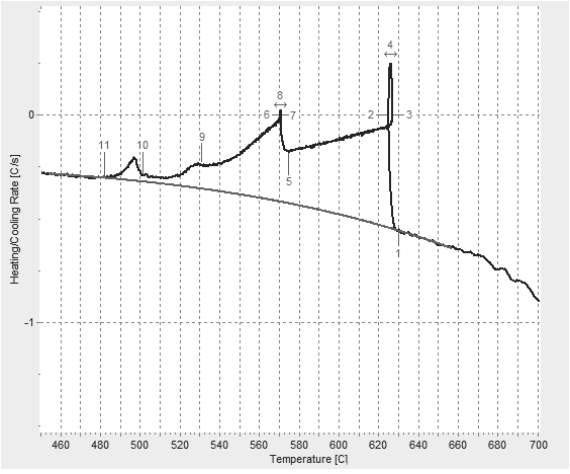

Fig. 2. First Derivative vs. Temperature Cooling Curve of a Nominal 5 wt.% Si and 1 wt.% Cu Aluminum Alloy with Overlaid Dynamic Baseline

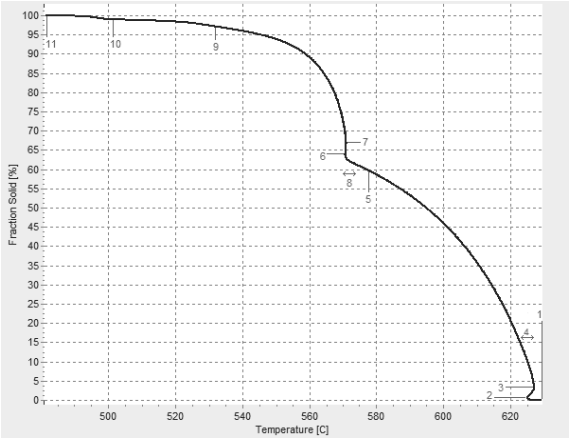

Fig. 3. Fraction Solid Curve of a Nominal 5 wt.% Si and 1 wt.% Cu Aluminum Alloy with Metallurgical Events Indicated

2. Literature review

2.1. Dynamic baseline

A variety of papers published over the past thirty-five years have presented many different techniques for experimentally determining the ***DBL*** equation for the solidification process. Some of these methods have been based on arbitrarily applied assumptions and are subject to different interpretations. A summary of selected techniques and a comparison of results were presented by Barlow and Stefanescu [11]; Kierkus et al. [12]; E. Fras et al. [13] and Emadi et al. [14]. These authors reviewed three distinct approaches to the ***DBL*** calculation:

1) Newtonian analysis;
2) Fourier analysis;
3) Empirical analysis with the assumption of one or three different heat transfer coefficients.

The University of Windsor initially developed a ***DBL*** for the AlTAP cooling cycle and later adapted it to the UMSA Technology Platform. The ***DBL*** concept presented in this report is based on the Newtonian model adopted by Stefanescu et al. [15-17] and other authors [9] for cooling curve analysis. The different paths taken to finalizing both AlTAP and UMSA ***DBL*** procedures is partially presented in [12].

In the past, users of Computer Aided Cooling Curve Analysis (**CA-CCA**) were able to obtain only limited information from the cooling curve and its first derivative. The primary reason was that the scientifically proven ***DBL*** curve was not available for the generation of reliable physical data comparable with other techniques including Differential Scanning Calorimetry (**DSC**). The conventional **CA-CCA** technique gathers data as follows:

1) A melt sample is poured into an open sand, graphite and/or steel test cup where it solidifies with a single, centered thermocouple recording the temperature (T_c).
2) The T_c is plotted against time to create a cooling curve.
3) Its first derivative is calculated.
4) Basic thermal data is determined.

More recently, this technique was refined by the addition of a second thermocouple positioned near the wall of the cup. According to proponents of this approach, recording the "wall" temperature (T_w) allows for more accurate thermal analysis results but unfortunately never precisely defines the distance from the wall [18-20]. This procedure, however, necessitates a substantially more complicated experimental setup. In addition, a recent study [21] suggests that the data provided by two or three thermocouples [22] may not be any more accurate than the single thermocouple technique provided that either the first or both, the first and second derivative of the T_c are used for analysis. Utilization of more than one thermocouple is fully justifiable for the many other types of analysis, including in-situ assessment of riser feeding efficiency, etc. [6].

The ***DBL*** equation calculation procedure presented in this paper requires that the lumped thermal capacity system being considered (i.e. the metal/alloy test sample, the cup and the thermocouple) complies with Newtonian cooling model requirements. This means that the temperature within the system must be a function of time only and be spatially uniform, or at least that the temperature gradient in any direction within the system must be negligible at any instant during the cooling/solidification process. These conditions are most closely satisfied when:

a) A thin-walled metal cup (including steel foil crucible for Al and Mg alloys) is used in conjunction with a low thermal inertia thermocouple in which only the tip is directly exposed to the melt. The shaft of the thermocouple is protected by a small diameter ceramic sheath. The small thermal mass of the cup and thermocouple is negligible in comparison with the test sample mass so the thermocouple can track the true temperature with minimal lag. This configuration limits the interference between the tested material, the cup and the thermocouple. The recorded cooling/heating curve thermal events are controlled by elimination of additional solidification front(s). This approach also allows for the unbiased analysis of the material's thermal data since the cup and thermocouple "heating and cooling" effects are negligible.
b) The cup is well insulated from both, the top and the bottom, for example, using low density ceramics. This secures the one- dimensional heat transfer mode.
   Note: Other carefully designed and verified test cups, thermocouples and experimental setups may also be sufficient for specific tasks. However, additional metallurgical factors may also have a considerable effect on the integrity of the cooling/heating curve analysis and must be considered. For example, an optimized melt sampling procedure will ensure unbiased test sample cleanliness (the type and level of gas and insoluble inclusions must be identical as in the furnace) but during the melting cycle the test sample must be protected in order to prevent oxidation and absorption of hydrogen.
c) The rate of cooling due to loss of energy from the cup to its surroundings should be limited by the Biot modulus (**Bi**) which is based on the thermal system's "characteristic dimension" and the "overall heat transmission coefficient". The value of ***Bi*** should not exceed 0.1.

Biot modulus is defined as:

$$Bi = VU/AK_{eff} \quad (1)$$

Where:

V - Volume of the cast sample (lumped system);
U - "Overall apparent heat transmission coefficient" between the cast test sample and its surroundings (lumped system) by all possible heat transfer modes (convection, conduction and radiation). ***U*** is a time dependent function;
A - Surface area of the cast test sample (lumped system);
K_{eff} - Thermal conductivity of the alloy.

The characteristic dimension can be defined as the ratio of the system volume to its outside surface area (i.e. the area of the system through which energy is lost to the surroundings). The overall heat transmission coefficient is based on the total thermal resistance between the temperature of the solidifying test sample (T_c) and the temperature of the surroundings (T_s, also sometimes

defined as T_∞). The requirement of Bi < 0.1 will hold for the majority of metals, alloys, metal matrix composites and experimental conditions including physically simulating lost wax and foam processes, sand and semi-permanent casting processes and other casting technologies.

Finally, during the solidification process of the test sample, the "apparent sensible thermal capacitance" of the system should not be temperature dependent. Once again, this is typically the case for most metals, alloys and metal matrix composites. Under the assumptions described above, the energy balance can be written in the form shown in Equation 2.

$$\rho C_p V \frac{d(T_c - T_\infty)}{dt} = -AU(T_c - T_\infty) + \frac{dQ_L}{dt} \quad (2)$$

Equation 2 can be re-written as the first derivative of a cooling curve as a function of time (dT_c/dt):

$$\frac{dT_c}{dt} = -(\frac{AU}{\rho C_p V})(T_c - T_\infty) + \frac{1}{\rho C_p V}\frac{dQ_L}{dt} \quad (3)$$

Equation 3 can also be presented in the form of Equation 3a:

$$\frac{dTc}{dt} = \frac{1}{\rho C_p V}\left[\ \frac{dQ_L}{dt} - AU(T_c - T\infty)\ \right] \quad (3a)$$

Where:

C_p - "Sensible apparent specific heat" (lumped system);

ρC_p - "Apparent sensible thermal capacitance" per unit volume (lumped system) expressed as a product of the alloy density (ρ) and its specific heat;

T_c - Temperature in the test sample center;

T_∞ - Temperature of the system surroundings, assumed to be constant and "known" for the experiment;

t - Time;

Q_L - The energy generation rate when sample/casting section changes its state from liquid to solid or vice versa (this quantity, also known as the latent heat, is positive during solidification and negative during the melting process).

The ***DBL*** equation is calculated using Equation 3 or 3a as a portion of the first derivative of a cooling curve between liquidus ($T_{c,liq}$) and solidus ($T_{c,sol}$) temperatures assuming absence of any metallurgical reaction(s). This condition is satisfied under the conditions in Equation 4.

$$\begin{aligned} &Q_L = 0 \\ &T_c \geq T_{c,liq} \ @\ t = t_{c,liq} \\ &T_c \leq T_{c,sol} \ @\ t = t_{c,sol} \end{aligned} \quad (4)$$

If the conditions in Equation 4 are taken into consideration, Equations 3 and/or 3a can be reduced to Equation 5, shown below.

$$\frac{dT_{CBL}}{dt} = (-\frac{AU}{\rho C_p V})(T_{cBL} - T_\infty) \quad (5)$$

Where:

T_{cBL} - Temperature of the ***DBL*** in the test sample center.

The above energy balance for the ***DBL*** portion can also be written as a rearranged Equation 5a while accounting for the liquid and/or solid single phase formed during cooling of the test sample or cast component section.

$$\frac{1}{T_{cBL} - T_\infty}\frac{d(T_{cBL} - T_\infty)}{dt_{cBL}} = -(\frac{AU}{\rho C_p V}) \quad (5a)$$

When solved, Equation 5 and the rewritten Equation 5a will determine the time dependent T_c before the solidification process has started and after it has been completed (as stated in Equation 4). Equations 5 and 5a are representative for the single phase states of the solidification or melting process (i.e. liquid or solid, Q_L = 0). On the right side of these Equations, only U (the overall heat transmission coefficient) is a time dependent function. The other variables grouped in the bracket on the right side are virtually constant or can be assumed to be constant without introducing significant error into the results. The right side of Equation 5a can be termed an "effective overall heat transmission coefficient" **U***. Therefore, the measured T_c, as a function of time, can exclusively define the $U(t)$ for given experimental conditions by fitting a polynomial using the least square method to the left side of Equation 5a.

It is commonly believed that the overall "apparent heat transmission coefficient" U cannot obey the same continuous function before and after solidification. However, several University of Windsor experiments using both industrially pure metals (aluminum and tin) and 319.2 and 356 aluminum alloys have shown otherwise. Close inspection of Equation 5 and 5a shows that only U is truly time dependent. In theory, the term ρC_p also depends on temperature and therefore is a function of time but the variation is so small that it can be treated as a constant. ρC_p term does not vary more than +/- 0.7% of its average value for aluminum alloys tested in the range of 800 and 400°C. Based on the measured T_c, the numerically determined dT_c/dt and the $U(T_c)$ function, dT_{cBL}/dt can be calculated if the right side of Equations 5 and/or 5a is fit as a polynomial in terms of T_c by using the least square method, resulting in Equation 6.

$$\frac{dT_{CBL}}{dt} = \sum_{i=0}^{n} a_i (T_{cBL})^n \quad (6)$$

In those cases where ρC_p is slightly temperature dependent, over the analyzed range of temperatures, this dependence is incorporated into the constants of the fitted polynomial (a_i).

Because dT_{cBL}/dt is a function of T_c only, the $U(T_c)$ is valid for all parts of the cooling curve in the whole range of T_c measurements. Therefore, the values of dT_c/dt can be determined

for all recorded values of T_c, which form the ***DBL*** Equation 7 shown below.

$$\frac{dT_{cBL}}{dt} = F(T_{cBL}) \tag{7}$$

This equation is clearly a function of time because T_c is time dependent.

2.2. Fraction solid

Many effects of CR/SR on the solidification process parameters, including the potential effect of f_s at the Dendrite Coherency Point (***DCP***), are presented in the literature [17,19,23-29]. At the ***DCP***, porosity, shrinkage and hot tearing start to develop. Earlier work at the University of Windsor proved that the f_s at the ***DCP*** is higher with an increased SR and thus prolongs mass feeding to a later point during the solidification process. This work showed that the thermal modification can be quantified using f_s curve parameters [7]. The in-situ thermal analysis of the complex cast component used to assess riser feeding efficiency is compelling evidence about the comprehensive capabilities of this technique to assist in metal casting technology optimization [6].

Some direct and in-direct methodologies used for determination of the f_s evolution during solidification processes are summarized and evaluated in terms of the advantages and limitations specific to certain applications [15,17,30-41]. The following most often utilized methods can be categorized as follows:

1. Thermal analysis techniques:
   - 1.1 Differential Scanning Calorimetry (DSC) and Differential Thermal Analysis (DTA).
   - 1.2 Computer Aided Cooling Curve Analysis (**CA-CCA**).
     - 1.2.1 ALTAP technology platforms (i.e. environmental, in-situ, etc.).
     - 1.2.2 UMSA technology platforms (i.e. vacuum, pressure, etc.).
2. Computational thermodynamic software packages for equilibrium and non-equilibrium solidification processes.
3. Quantitative metallography on microstructures quenched from the semi-solid state.
4. Ultrasonic monitoring by measurement of propagation speed of ultrasonic waves.
5. Measurement of electrical resistance/magnetic permeability.
6. Measurement of mechanical response by indentation, back extrusion, etc.
7. Measurement of electrical potential difference or uni-axial flow stress that mathematically relates the obtained values to fraction solid.

Please note that since the focus of this paper is on CA-CCA f_s methodologies, only some of the above mentioned methods are expanded in more detail.

DSC and DTA have been used for the determination of f_s [7]. One of the limitations of these two techniques include the restriction to very small (mg range) test samples that are not fully representative of the cast component's structures. As-cast structures often exhibit macro-segregation of alloying and impurity elements and contain inclusions, gas and shrinkage pores as well as undesirable macroscopic constituents, etc. that affect measured thermal data. These effects are not fully understood and cannot be easily quantified using DSC/DTA methodologies. DSC and DTA are, however, indispensible for the benchmarking of on-line industrial and laboratory thermal analysis data (i.e. Latent Heat of Fusion) of complex materials tested under 'ideal" conditions using **CA-CCA** methodologies.

The literature suggests a number of f_s models using equilibrium phase diagram data, which are summarized in Table 2, #1-3. These models are based on fundamental solidification data of simple alloy systems. Because of the highly complex nature of industrial alloys, processes and cast components, many questionable and simplified assumptions are made in these models (see comments in Table 1). Often these models yield f_s data for only some solidification events and are not fully representative of calibrated **CA-CCA** data (i.e. undercooling events). Using simplified models for applied engineering solutions can also often require time consuming iterative approaches (both theoretical and experimental) to account for the actual industrial environment processing conditions. For example, the Scheil equation has quite severe restrictions when applied to multi-component alloys and can be applied only to dendritic solidification [34]. It is critical for the understanding and quantification of industrial alloy phase transformations, processes and cast components properties that all solidification events be taken into account.

According to [42-43] utilization of thermodynamic modeling sufficiently limits the Scheil-Gulliver assumption and leads to "good results for much of the solidification range."FactSage, Thermo-Calc and JMatPro are three of the most powerful packages that use Scheil-Gulliver isothermal step modeling. The first two tested packages render good Latent Heat (***LH***) data for the non-equilibrium solidification process [19].

This paper revealed that the ***LH*** calculated using statistical methods, Si_{EQ} methodology, FactSage, and Thermo-Calc renders comparatively small average error. The Coefficient of Correlation (R^2) with the DSC data is significantly higher for the first two methods (R^2=0.97) vs. approx. 0.90 for the latter two. More in-depth work is needed to compare thermo-physical solidification characteristics assessed by the ***CA-CCA*** and modeling methodologies while considering all the parameters describing metallurgical reactions that are relevant to the industrial environment. The use of the computational software packages is limited by the thermodynamic databases used in the calculations.

Highly competitive industries like transportation require rapid R&D tools for commercialization of proven materials, technologies and cast components. Therefore, further development and commercialization of the novel engineering tools (i.e. AlTAP and UMSA) capable of addressing industrial requirements is of utmost importance. The wide range of scientifically and industrially relevant technical capabilities of the UMSA and AlTAP, developed by the University of Windsor, make them very attractive engineering tools for determining various thermal characteristics including f_s [6-7,10].

The DSC method of partial areas determines experimentally approximated f_s data, making the assumption that the heat of melting is independent of the temperature (Table 2, #5).

Methods of modeling non-equilibrium solidification processes of complex industrial alloy systems, shown in Table 2, #7-8, do not have the previously mentioned limitations and are based on experimental AlTAP and UMSA cooling curve data [44].

The literature also presents a quantitative metallography technique for determination of the volume fraction of phases formed prior to rapid quenching from mushy zone temperatures [30]. This technique requires the use of small test samples in order to preserve the structure present at a given temperature of interest. Both small test samples and rapid quenching rates minimize structural transformation(s) during this operation and thus maximize the accuracy of this measurement procedure. This technique is not suitable for on-line measurements. In addition, this technique is very time consuming because it requires high spatial resolution data in the given region of interest. A rapid quenching method presented by J. Wannasin et al. which takes into account the growth layers of the solid phase(s) allows for the actual pre-quenching f_s to be determined [31].

Four prominent f_s prediction models based on the experimental thermal analysis data can be used for f_s determination at any point during the solidification of the test sample or cast component. These are: the Su and Tsai model [35], the Fras et al. Fourier's model [13] the Huang source/sink algorithm for modeling phase changes [37] and the W. T. Kierkus and J.H. Sokolowski Newton ***CA-CCA*** model [11,12]. Unfortunately, most of these methods have essential and important limitations. They require that at least one of the following be explicitly known:

1) Accurate and detailed information regarding thermal properties of an alloy and mould material (as function of temperature) and detailed knowledge of the heat transfer rate between the cast component and the mould,
2) Knowledge of the heat transmission coefficient from the casting-mould system to the surroundings and recorded temperature history of the casting,
3) Knowledge of the thermo-physical properties of the casting-mould-surroundings thermal system.

Due to the fact that the geometrical and thermal complexity of the casting-mold "system" (i.e. castings and mold material change their physical properties with the temperature and time) this information is not directly available to the investigator, so in order to perform analysis, these properties must be assumed on an *a priori* basis. While it is possible to correct erroneous assumptions on a trial-and-error basis, the accuracy of these attempts has thus far been questionable. In addition, these analyses have been lengthy and computationally complex, which limits their use in practical industrial situations.

The first two methods require either accurate knowledge of the thermal properties of the cast alloy or the heat transmission coefficient from the casting to its surrounding while the third one uses both the recorded temperature of the casting and physical properties of the mold. However, the ***CA-CCA*** methodology is able to predict the f_s of the cast component section(s) in the semi-solid region by introducing the concept of a single function heat transmission coefficient based on the casting temperature. In the case of the single phase (liquid or solid) cooling stages of the test sample or cast component, the energy balance equation is presented in Equation 1. Once the unique function of the multimode heat transmission coefficient **U** is expressed in terms of measured temperature $\mathbf{T_c}$ and its derivative $\mathbf{dT_c / dt}$ (Equation 6), it is possible to express the f_s for any temperature between equilibrium and non-equilibrium $\mathbf{T_{Liq}}$ and $\mathbf{T_{Sol}}$. It should be noted that the ***DBL*** determination method described in Section 2.1 can also be used to create input for the methods described in [13] and [35].

2.3. Development of the silicon equivalent (Si_{EQ}) algorithm

The liquidus and solidus temperatures of the Al-Si phase diagram decrease uniformly with the increase in the amount of silicon and reaches the minimum at eutectic composition (12.2 wt.%) which can be seen in Figure 4. The same behavior can be observed in the liquidus and solidus lines in most of the binary eutectic type of aluminum alloys which inspired the development of an equivalency algorithm [46,47].

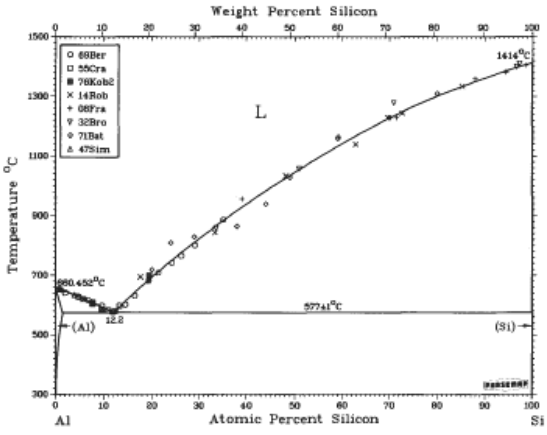

Fig. 4. Aluminum Silicon Binary Phase Diagram [48]

Mathematically, liquidus and solidus lines of these binary systems can be accurately expressed in second order polynomial form as shown in Equations 8a and 8b.

$$T^{Al\text{-}Xi}{}_{LIQ} = A - B \cdot Xi - C \cdot Xi^2 \quad [^oC] \qquad (8a)$$

$$T^{Al\text{-}Xi}{}_{SOL} = A - D \cdot Xi - E \cdot Xi^2 \quad [^oC] \qquad (8b)$$

Where:

Xi content of the alloying element in wt.%.
A is the melting point of pure aluminum 660.452°C.
B, C, D, and E are polynomial coefficients.

The liquidus and solidus line for the Al-Si binary system can be expressed as shown in Equations 9a and 9b.

$$T^{Al\text{-}Si}{}_{LIQ} = 660.452 - 6.11 \cdot Si - 0.057 \cdot Si^2 \quad [^oC] \qquad (9a)$$

$$T^{Al\text{-}Si}{}_{SOL} = 660.452 - 52.8 \cdot Si - 3.70 \cdot Si^2 \quad [^oC] \qquad (9b)$$

Table 2.
Selected f_s models for equilibrium and non-equilibrium solidification processes [14,44,45]

#	f_s MODELS	COMMENTS
1	**LINEAR** $f_s = \frac{T_{liq} - T}{T_{liq} - T_{sol}}$ T_{liq}- Liquidus temperature T_{sol}- Solidus temperature T - Instantaneous temperature	Latent heat of fusion is assumed to vary linearly between T_{liq} & T_{sol} temperatures. This model has no theoretical basis, but is frequently used due to its simplicity.
2	**LEVER RULE** $k = \frac{T_m - T_{liq}}{T_m - T_{sol}}$ $f_s = \frac{1}{1-k} \cdot \frac{T_{liq} - T}{T_m - T}$ k - Distribution coefficient of binary alloy T_m - Melting temperature of pure metal	Equilibrium solidification is assumed to progress very slowly and the solid and liquid phases coexist in thermodynamic equilibrium in the mushy zone. f_s is determined by the lever rule.
3	**SCHEIL** $f_s = 1 - \left(\frac{T_m - T}{T_m - T_{liq}} \right)^{\frac{1}{k-1}}$	It is assumed that no solute diffusion occurs in the solid phase (which results in segregation) and also that the liquid is perfectly homogeneous (assumed complete diffusion).
4	**GRAIN NUCLEATION** $f_s = 1 - \exp\left(-\frac{4}{3} \cdot \pi \cdot R^3 \cdot N \right)$ R-Average grain radius N-Average grain density	The calculation of f_s is based on the grain nucleation law and on the assumption that the shape of the grains is spherical.
5	**DSC METHOD OF PARTIAL AREAS** $f_s(T) = 1 - (1/m\Delta H)Q(T)$ $Q(T)$ - Heat absorbed from melting to T m - Mass of the sample ΔH - Heat of melting	f_S equation is an approximation by assuming that, the heat of melting is independent of the temperature and thus the composition of the solid phase is linearly proportional to the amount of the melted alloy.
6	**FOURIER METHOD** $f_S(t) = \frac{1}{L} \int_{t_s}^{t} \left(\frac{\partial Q}{\partial t} \right)_t (t)\, dt$ L - Latent heat Q - Latent heat of solidification	Fourier's model considers the effect of thermal gradient (at least two thermocouples are needed) during solidification and assumes that the heat transfer takes place by conduction only. Cylindrical or spherical samples are used.
7	**SEGMENTATION MODEL - 319 alloy** $f_S^{\ I} = (T_{liq} - T)/(T_{liq} - T^{AlSi}_{E,G})^{n1} f_S^{\ AlSi}$ $f_S^{\ II} = f_S^{\ AlSi} + (T^{AlSi}_{E,G} - T)/(T^{AlSi}_{E,G} - T^{AlCu}_{E,G})^{n2} (f_S^{\ AlCu} - f_S^{\ AlSi})$ $f_S^{\ III} = f_S^{\ AlCu} + (T^{AlCu}_{E,G} - T)/(T^{AlCu}_{E,G} - T_{sol})^{n3} (100 - f_S^{\ AlCu})$	f_s vs. temperature curve is modeled based on three segmented experimental cooling curve thermal events for the whole solidification range and varying SR. Agreement of modeled and experimental data R^2=0.99.
8	**NEWTONIAN HEAT BALANCE** $f_S(T_c) = \frac{\int_{T_{Liq}}^{t} \left(\frac{dT_c}{dt} - \frac{dT_{cBL}}{dt} \right) dt}{\int_{T_{Liq}}^{T_{Sol}} \left(\frac{dT_c}{dt} - \frac{dT_{cBL}}{dt} \right) dt}$	f_s is calculated by determining the cumulative area between the dT_c/dt of the cooling curve, and the dT_{BL}/dt (BL). This methodology is utilized for ALTAP and UMSA measurements and post-processing f_s analysis.

Visual comparison of the Al-Si binary system with any other Al-Xi eutectic system shows a high degree of similarity. All binary systems will decrease the liqidus temperature of the alloy until the eutectic point, at which point it will rise again. The main difference is in the fact that compared to Si, a different concentration of Xi is required in order to produce an equivalent change of the melting point of aluminum alloy. Based on this following relationship can be established:

$$Si^{Xi}_{EQ,T=CONST} = Si - Xi \quad [wt.\%] \qquad (10)$$

Where:

$Si^{Xi}_{EQ,T=CONST}$ is the isothermal concentration difference between Si and Xi alloying elements.

This relationship can be applied to calculations for both hypoeutectic and hypereutectic alloys. Since silicon is the major alloying element for the 3XX series of aluminum alloys, it is chosen as the reference element. It also has the most significant influence on the casting properties of these alloys (e.g. fluidity and shrinkage).

Because the isothermal concentrations of Si are usually smaller than corresponding concentrations of the observed Xi element, values for $Si^{Xi}_{EQ,T=CONST}$ in Equation 10, are given in absolute value.

Taking into consideration the temperature range between the melting temperature of pure aluminum and the eutectic temperature of an observed binary system, the following relationship can be established between Si^{Xi}_{EQ} and the concentration of alloying element, Xi (Equation 11).

$$Si^{Xi}_{EQ} = a_0^{Xi} + b_0^{Xi} \cdot Xi + c_0^{Xi} \cdot Xi^2 \quad [wt.\%] \qquad (11)$$

Where:

a_0^{Xi}, b_0^{Xi} and c_0^{Xi} are polynomial coefficients.

Xi is the concentration of the alloying element in wt.%.

The Si_{EQ} for major (Cu, Fe, Mg, Mn and Zn) and minor (Ca, Ni, Cr, etc.) alloying elements as well as some impurity elements (Pb, Sn, and Bi) modifiers, grain refiners (Sr, Na, Sb, Ti and B) and even gases (H_2 and N_2) can be calculated as the sum of individual contributors (ΣSi^{Xi}_{EQ}) plus the effect of silicon itself:

$$Si_{EQ} = Si + \Sigma Si^{Xi}_{EQ} \quad [wt.\%] \qquad (12)$$

The characteristic temperatures for multi component 3XX aluminum systems can be calculated using the following Equations 13-15.

$$T^{Al\text{-}Si\text{-}\Sigma i}_{LIQ} = 660.452 - 6.11 \cdot Si_{EQ} - 0.057 \cdot Si_{EQ}^2 \quad [^oC] \qquad (13)$$

$$T^{AlSi}_{,NUC,\,E} = 660.452 - ((6.11 \cdot Si_{EQ} + 0.057 \cdot Si_{EQ}^2) \cdot 12.3/Si \quad [^oC] \qquad (14)$$

$$T^{Al\text{-}Si\text{-}Cu}_{NUC,\,E} = T_{LIQ} - (6.11 \cdot Si_{EQ} - 0.057 \cdot Si_{EQ}^2) \cdot 12.3/Si \quad [^oC] \qquad (15)$$

In later calculations in this paper, Cu is not considered in Si_{EQ} calculations for the following two reasons. First, the main alloying elements are Si and Cu. Other elements expressed as Si_{EQ} are present in relatively low amount (10^{-2} wt.%) and have narrow ranges. Therefore, for this general analysis it is convenient to present the f_s data only as a function of Si and Cu as two main alloying elements. Second, for the highly alloyed melts (i.e. containing high levels of Cu and Si) some metallurgical characteristics could require more in-depth analysis to account for the interaction(s) between Si and Cu elements that are outside of the scope of this paper.

3. Baseline analysis

3.1. Analytical procedure for calculation of the Dynamic Baseline

The Newtonian model requires that the temperature within a system can be assumed as spatially uniform and that the system's thermal properties can be considered temperature independent. These requirements hold for the majority of metals and alloys under most conditions during heating and solidification processes (regardless if one is considering a test sample or an actual industrial cast component). Therefore, the only temperature dependent variable that remains in the energy balance equation is the overall heat transmission coefficient ***U***. An extensive University of Windsor study [12] confirmed that an effective solution of the simplified energy equation can be found using a function fitting technique even if ***U*** remains explicitly unknown.

The ***DBL*** equation may be calculated by using the following steps:

1) During the cooling process, record the test sample temperature as a function of time, $T_c\,(t)$.
2) Determine the first time derivative of this temperature, dT_c / dt.
3) Fit a polynomial, $F(T_c)$, in the order ≥ 2 to the portions of the solidification temperature range ($T_{liq} < T_c < T_{sol}$) for the hypothetical single phase. A third order polynomial is sufficient to express the function and to obtain a very high correlation coefficient (R^2).
4) Calculate the function $F(T_c)$ for all temperatures recorded in the experiment. The resultant function, dT_{cBL} / dt is the calculated ***DBL***.

DBL equation calculation is performed automatically in the AlTAP/UMSA software and can be visualized as an overlay on the first derivative of the heating/cooling curve.

Once the unique function of the multimode heat transmission coefficient **U** is expressed in terms of measured temperature $\mathbf{T_c}$ and its derivative $\mathbf{dT_c / dt}$, it is possible to express the fraction solid for any temperature between equilibrium and non-equilibrium $\mathbf{T_{Liq}}$ and $\mathbf{T_{Sol}}$. Obviously, the $\mathbf{f_S}$ = 0.0 for $\mathbf{T_c > T_{Liq}}$ and **fs** = 1.0 for $\mathbf{T_c < T_{Sol}}$.

3.2. Visual representations of the DBL

Visual representations of the above described experimental and analytical steps leading to the ***DBL*** for the 319.2 aluminum alloy is presented in Figures 5-8 below.

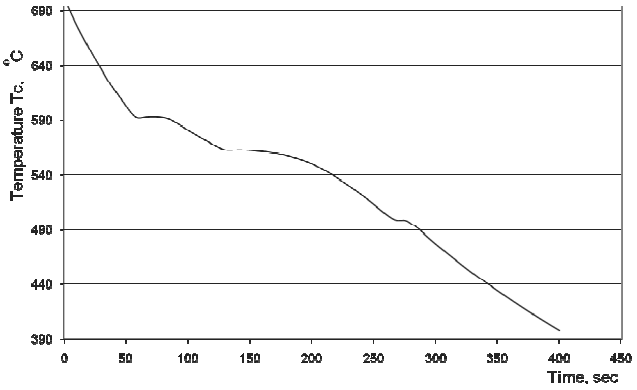

Fig. 5. Cooling Curve for the 319.2 Aluminum Alloy

Figure 5 shows a temperature vs. time cooling curve for the 319.2 aluminum alloy. This curve was obtained during an AlTAP experiment performed in the University of Windsor's Metal Casting and Post-Processing Technology laboratory. A graphite crucible (65 mm in height and 50 mm in diameter, and walls/bottom 5 mm thick) with an insulated top and bottom was used to contain the molten sample. The ambient temperature in the lab during measurement was approximately 25°C.

Figure 6 presents the first time derivative (dT_c/dt) of the temperature T_c as a function of time. The ***DBL*** polynomial given in Equation 6 was fitted between the non-equilibrium liquidus and solidus temperature points (semi-solid region) using liquid melt and solid sample portions of the dT_c/dt curve. According to the dT_c/dt curve, the sample remains liquid until approx. 50 sec after pouring and solidifies after approx. 275 sec followed by a period of cooling.

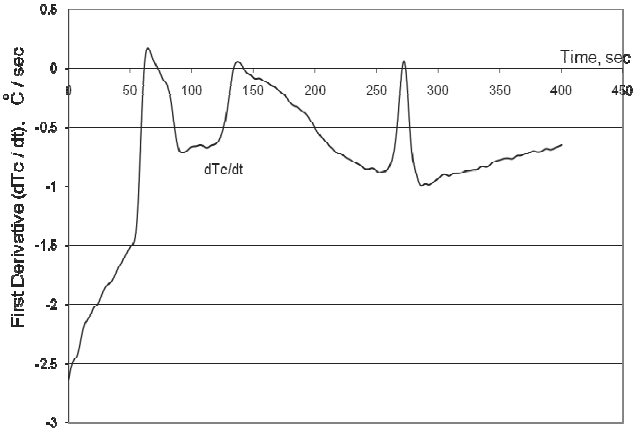

Fig. 6. First Derivative of the Cooling Curve for the 319.2 Aluminum Alloy

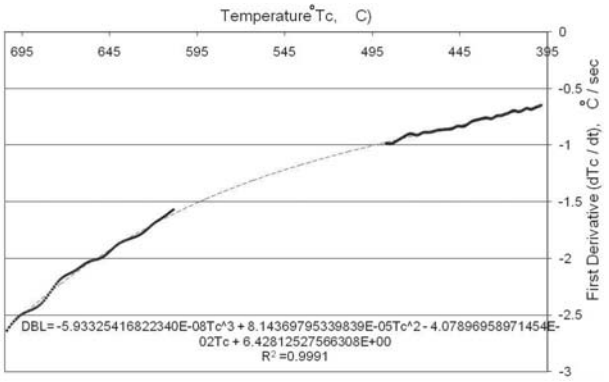

Fig. 7. Regression Equation of the Dynamic Baseline (***DBL***) for the 319.2 Aluminum Alloy

Figure 7 illustrates the results of the ***DBL*** fitting for the dT_c/dt as a function of T_c. The regression of the ***DBL*** equation is given at the bottom of this Figure. When third order polynomials were used for ***DBL*** determination, an excellent fit was obtained (R^2 = 0.9991) over a temperature range of T_c > 610°C and T_c < 500°C.

Figure 8 depicts the ***DBL*** overlaid on the full first derivative from Figure 6. It is clear that the ***DBL*** curve is only temperature dependent before the start of the solidification process and after its completion (where it very closely follows the first derivative of the cooling curve). Therefore, it can be assumed that the difference between the first derivative of the experimental cooling curve and the analytically fitted ***DBL*** at any given time represents the heat of the metallurgical reactions generated within the solidifying test sample at that point.

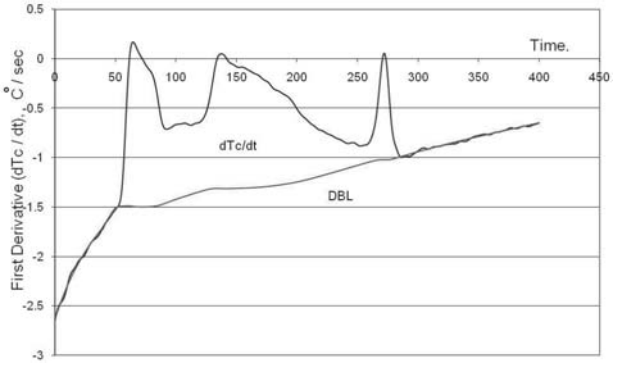

Fig. 8. First Derivative of the Cooling Curve and the Dynamic Baseline (***DBL***) for the 319.2 Aluminum Alloy

Similar experiments were performed on tin (99.95% pure) over a wide temperature range, the results of which are shown in Figures 9-12. These figures illustrate the ***DBL*** concept where the dT_c/dt can be plotted vs. time or temperature and can be utilized for detailed analysis of metallurgical characteristics.

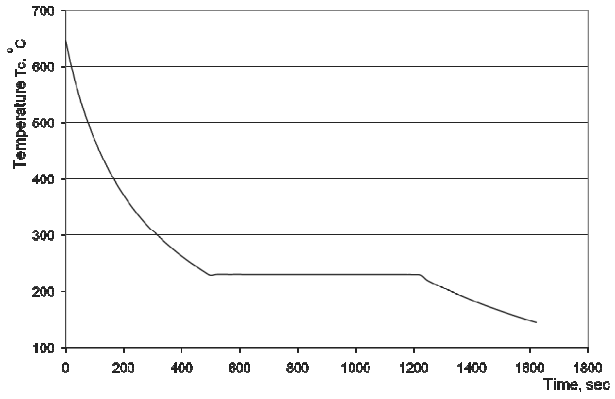

Fig. 9. Cooling Curve for Tin with a Purity of 99.95%

Evidence for the Newtonian ***DBL*** concept can be seen in the experimental and processed data from an AlTAP experiment on tin. The sample was heated to approximately 415°C above the solidification temperature and allowed to cool to room temperature in a natural heat exchange environment. The large temperature range was necessary in order to prove that the ***DBL*** curve provides a good fit for the data (R^2=0.9997). The experimental first derivative of the cooling curve is shown in Figure 12.

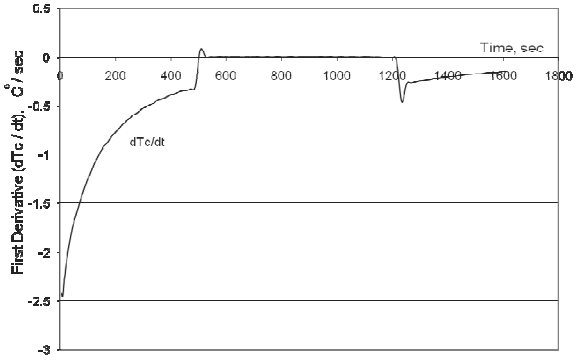

Fig. 10. First derivative of the Cooling Curve for tin with a purity of 99.95%

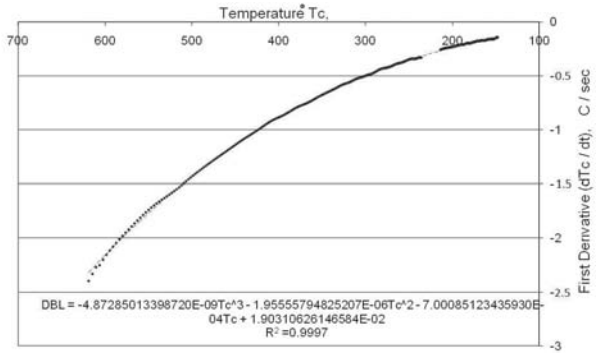

Fig. 11. Regression equation of the Dynamic Baseline (***DBL***) for tin with a purity of 99.95%

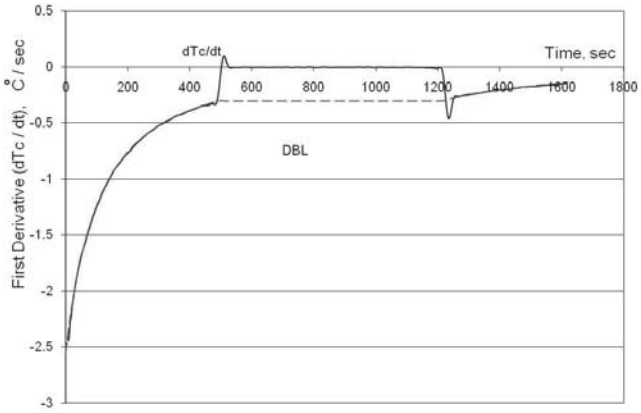

Fig. 12. First derivative of the Cooling Curve and the dynamic Baseline (***DBL***) for pure tin

The following observations can be made by analyzing the data shown in Figures 9 to 12:

- In Figure 9, prior to the bulk melt solidification process (approx. 500 sec from the beginning of the melt cooling process), the tin experienced an undercooling of approximately 1.7°C followed by temperature recalescence. The small degree of undercooling indicates the absence of a suitable number of solid nuclei. Therefore, the liquid melt cooled below its real solidification temperature. The nucleation temperature of the first formed dendrites (i.e. initiated by the inclusions) resulting from the rapidly released latent heat of fusion is 229.6°C. The dendrite nucleation event is also manifested by the rapid deceleration of the Solidification Rate (SR) from approx. -0.3°C/sec and creation of the exothermic peak having a maximum SR of approx. +0.1°C/sec at approx. 500 sec. As the nucleation begins, the latent heat of fusion is released causing an increase in the melt temperature. After temperature recalescence the sample remains isothermal for approx. 700 sec until the solidification process is completed.
- The isothermal plateau during tin's solidification has an average temperature of 231.305°C. This compares well to the Fixed Point Temperature for Calibration for pure tin provided by the National Institute of Standards and Technology (NIST), which is 231.928°C [49].
- Figure 12 shows the dT_c/dt and fitted ***DBL*** curves. During the solidus isothermal plateau event, the $dT_c/dt = 0$ while the ***DBL*** is straight and parallel to the first derivative.

The very small undercooling and the good comparison to NIST standards indicate that the thermal analysis equipment is calibrated and scientifically-based experimental and analytical procedures were utilized. In addition, the superimposed third polynomial order ***DBL*** function on the first derivative of the cooling curve in the function of very wide temperature range demonstrates a "perfect analytical ***DBL*** link" between the tin's liquid and solid states (Figure 12).

Further AlTAP experiments were also conducted using pure aluminum (99.99% Al) and aluminum alloy 356. The computed baselines in these experiments also showed excellent correlation to the experimental data. The R^2 was 0.9968 for the 'pure' aluminum and 0.9989 for the 356 aluminum alloy.

Additional AlTAP and UMSA work on a wide range of aluminum and magnesium cast alloys fully confirmed the abovementioned observations as far as the ***DBL*** quality is concerned. Benchmarking of the AlTAP and UMSA thermal data (based on the ***DBL*** equation including Latent Heat of Fusion) with DSC results revealed excellent agreement.

Figure 13 shows a complete UMSA heating and cooling cycle. It is worth pointing out the fact that significant shifting of the semi-solid reactions takes place during the melting and solidification processes (i.e. 48°C for non-equilibrium test sample processing). The pronounced peak at approx. 300°C is associated with a solid state metallurgical reaction resulting from the long natural ageing process.

The next section, pertaining to the methodology of the fraction solid determination, will provide details about metallurgical experiments performed on a wide range of aluminum alloys during which a large collection of thermal data (including f_S) was gathered.

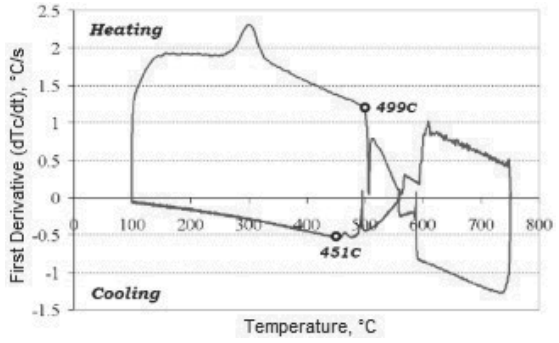

Fig. 13. UMSA first derivatives of the heating and cooling curves for the 319.2 alloy test sample

4. Fraction solid analysis

4.1. Determination of fraction solid using the newtonian CA-CCA model

The amount of f_s is directly proportional to the amount of **LH** evolved during the solidification process. The amount of **LH** can be calculated as the integrated area between the first derivative of recorded temperature, dT_c/dt and the ***DBL***, dT_{cBL}/dt. ***DBL*** represents the hypothetical first derivative of a cooling curve without phase transformations. Therefore, the method of ***DBL*** formulation (presented in Section 2.1) offers a simple way to determine f_s as a direct function of the recorded test sample temperature. This method uses post-process cooling curve analysis and requires the investigator to make practically no specific assumptions beyond the one made in the Newtonian model. This methodology is utilized for AlTAP and UMSA measurements and post-processing f_s analysis for the near-equilibrium and non-equilibrium processes.

Calculation of the fraction solid (f_s) as a function of the temperature T_c follows the relationship expressed in Equation 16.

$$f_s(T_c) = \frac{\int_{T_{Liq}}^{t}\left(\frac{dT_c}{dt} - \frac{dT_{BL}}{dt}\right)dt}{\int_{T_{Liq}}^{T_{Sol}}\left(\frac{dT_c}{dt} - \frac{dT_{BL}}{dt}\right)dt} \tag{16}$$

It should be obvious that $f_s(T_c)$, as calculated from this equation will assume the following values:

f_s in Equation 16 can be also expressed in the alternate form, shown in Equation 17, when the specific heat (C_p) and the latent heat of solidification (**L**) are known.

$$f_s(T_c) = \begin{cases} 0 \rightarrow T_c \geq T_{liq} \\ 0 < f_s < 1.0 \rightarrow T_{sol} < T_c < T_{liq} \\ 1.0 \rightarrow T_c \leq T_{sol} \end{cases} \tag{17}$$

Review of metal casting papers and handbooks indicates that the C_p and **L** data for the industrial alloys is not fully reliable. Therefore, in the case of C_p and **L** data uncertainty, the methodology expressed in Equation 3 is a better approach for determination of the unbiased f_s characteristics.

$$f_s(T_c) = \frac{Cp}{L}\cdot\int_0^t\left[\left(\frac{dT}{dt}\right)_c - \left(\frac{dT}{dt}\right)_{BL}\right]dt \tag{18}$$

4.2. Comparison of the literature and the authors' f_s data

It is difficult to compare the results of various fractions solid and temperature dependent analyses presented in the literature. Such comparisons are at best imprecise and do not allow for certainty of the conclusions. This is because the results of such analyses (as presented in [24-28]) depend in large part on the accuracy of the assumptions made by the researchers. To reproduce their results it was necessary to specify alloy compositions, experimental conditions and the geometry of their experimental systems. Variance was also introduced by differing sample cooling rates and measurement error. Unfortunately, information about most of these factors was not specified in the aforementioned publications. Therefore only approximate comparisons can be made between previous work and the results of the present study.

A striking example of these difficulties is presented in Figure 14. This figure compares the results of an experiment performed on the AlTAP at the University of Windsor and information gathered by Chen et al [25]. Both sets of experiments used "near pure" aluminum (99.95% purity in this study, unspecified purity in [34]). Nonetheless, substantial differences are visible at the beginning and end of solidification. The f_s curve from [34] does not exhibit the same undercooling and temperature recalescence. Recorded average T_c is 658.92°C and 657.32°C for the University of Windsor and [34] respectively, while the fixed point temperature for calibration using pure aluminum provided by NIST is 660.452°C [48]. The difference in cooling rates between the experiments, 1.6°C/s in [25] and 3.0°C/s for the

University of Windsor test, as well as the purity of the tested aluminum melt would be expected to create some differences.

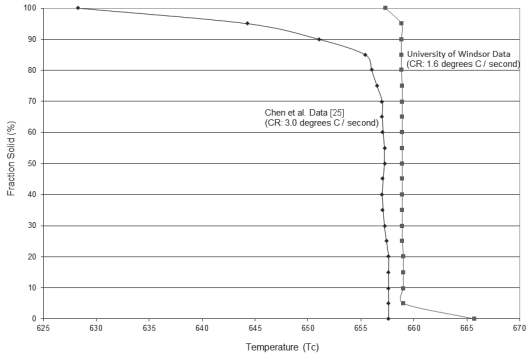

Fig. 14. Solidification of Near Pure Aluminum at Moderate Cooling Rates

Figure 15 shows f_s vs. temperature plot based on the dT_c/dt curve and ***DBL*** calculated as shown in Figure 9 for industrially pure tin. Undercooling of 1.7°C at 0.29% f_s was observed, while the recalescence to the T_{sol} temperature took place at 3.88% f_s. The vertical rise of the f_s to 100% at the isothermal temperature indicates that the sample is a pure substance.

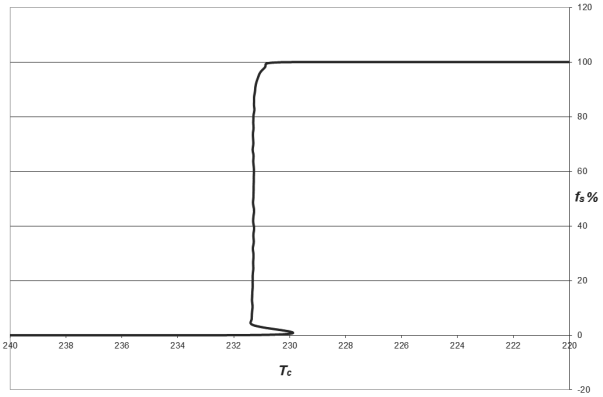

Fig. 15. Fraction Solid Curve for Industrially Pure Tin

Figures 16-19 present results of University of Windsor laboratory experiments on aluminum alloy 356 and comparisons with data taken from the literature [9,11,18,25] including the commonly used Scheil equation (for determination of the solid fraction temperature function). The presented fraction vs. solid temperature functions are labeled with the Solidification Rates (SR, °C/s) at which the experiments were run.

In order to rapidly benchmark the f_s data from various sources, the calculated Scheil f_s plot is used as the "theoretical reference". The Scheil f_s vs. temperature function consists of two distinct regions:

1. The curve starts at the $\mathbf{T_{liq}}$ (611.4°C, $\mathbf{f_s}$=0%) and continues as a smooth function up to the AlSi eutectic reaction (567.3°C, approx. 70% $\mathbf{f_s}$).
2. The f_s vertical isothermal jump at 567.3°C corresponds to the AlSi eutectic simultaneous nucleation and growth events starting at approx. 70% f_s and continuing to 100%.

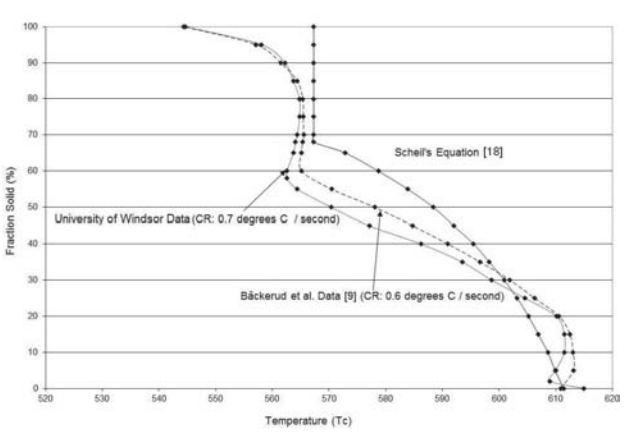

Fig. 16. Solidification of A356 Alloy at Medium Cooling Rates

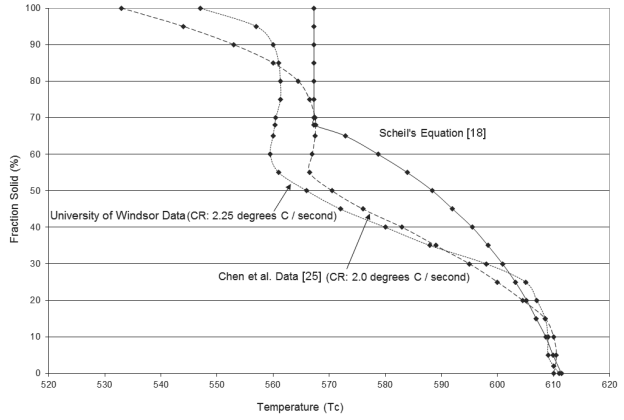

Fig. 17. Solidification of A356 Alloy at Moderate Cooling Rates

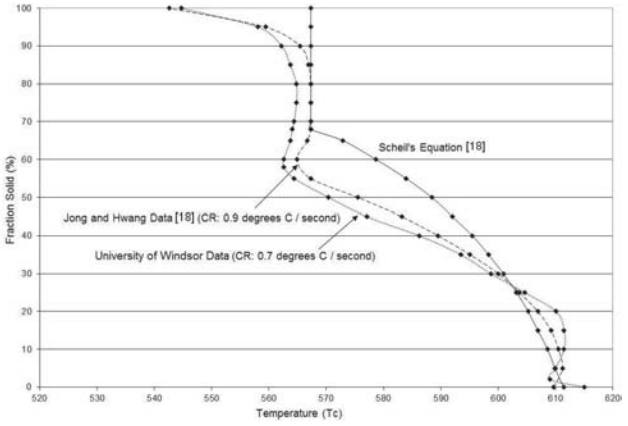

Fig. 18. Solidification of A356 Alloy at Medium Cooling Rates

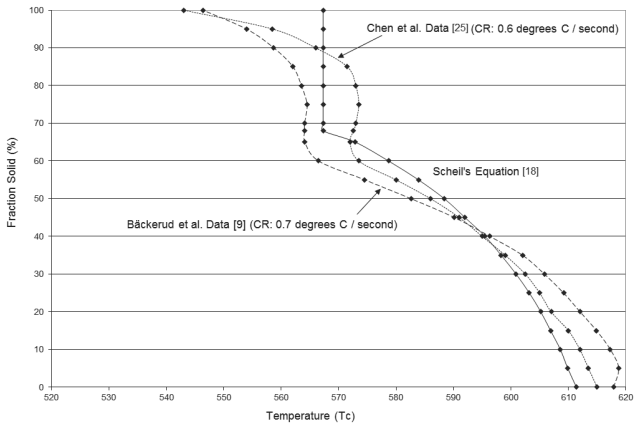

Fig. 19. Solidification of A356 Alloy at Medium Cooling Rates

According to the **CC-CCA** interpretative methodology, the equality of the following temperatures $T^{AlSi}_{E\ NUC} = T^{AlSi}_{E\ MIN} = T^{AlSi}_{E\ G} = T_{Sol}$ = 567.3°C is an assumption in the Scheil f_s model. It is also notable that the f_s at the start of isothermal rise is approx. 10% higher in comparison with the experimental curves. In addition, the Scheil f_s curve exhibits a very narrow solidification range ($T_{liq} - T_{sol}$) of 43.5°C in comparison with the experimental range of 70 to 78°C (depending on the data source and experimental conditions).

Closer inspection of the results presented in Figures 16 to 19 allow the following observations to be made:

1. All f_s curve data for the SR of 0.6 to 2.25°C/s indicate the start of nucleation for the αAl (the dendrite network) at the average temperature of 614°C.
2. Only f_s curves generated at the University of Windsor show undercooling during formation of the aluminum dendrites (2.2°C at SR = 0.7°C/s and 1.8°C at SR = 2.25°C/s respectively) and recalescence.
   i. Bäckerud's fs curve in Figure 19 exhibits a "temperature maximum" of 2.3°C (5% f_s) which does not have any physical justification.
   ii. Taking into consideration the limitations of the Scheil model (i.e. equilibrium solidification), its lack of undercooling is understandable*.
3. The experimental f_s curves show the AlSi eutectic nucleation point and undercooling parameters as well as the gradual f_s rise to the solidus temperature that corresponds with 100% f_s.
4. $T^{AlSi}_{E\ NUC}$ is indicated at the average temperature of $565^{+/-5}$ °C and the average value of $f_s = 60^{+/-4}$ % which is close to the "rigidity point "of the 356 alloy.
5. Comparison of the f_s versus temperature functions taken from [9,18,25] with University of Windsor data indicate that the maximum temperature differences are 9°C (75-80% f_s) at lower SR and 8°C (60-65% f_s) at higher SR. These differences and the one below should be considered substantial:
   i. The maximum difference of 14°C at Tsol for 100% fs is observed for the higher SR, see Figure 17.

***Note:** Undercooling events are associated with various metallurgical reactions and their characteristics are used for determination of several cast component properties including: Grain Size, Silicon Modification Level (SiML) and others. Integrity of the metallurgical information requires that the identical undercooling characteristics must be present on both the f_s curve and the cooling curve otherwise thermal analysis data cannot be considered to be fully reliable and can lead to erroneous outcomes.

4.3. AlTAP analysis of fs of 3XX aluminum alloys with variable Si and Cu content

In order to demonstrate characteristics of the f_s in function of temperature, experimental casting alloys with twelve different melt chemistries were selected having nominal chemical compositions with combinations of 5, 7, 9 and 11 wt% Si and 1, 2 and 4 wt% Cu and covering a wide range of the 3XX alloy system. The overlay of Si and Cu matrix of experimental 3XX alloys is presented in Figure 20 and Table 3 gives their detailed chemical compositions determined by Optical Emission Spectroscopy (OES). In order to simplify the f_s data presentation, Si and non-Si elements are expressed as a combined Silicon Equivalency (Si_{EQ}) content calculated according to Section 2.3. Please note that Cu is excluded from the present calculations since it is a major alloying element and its individual effects are of interest to this study.

Twelve 3XX alloys were produced at the Nemak Engineering Centre, Windsor, Ontario, Canada by mixing 99.99% pure Al and two master alloys: Al49wt%Si and Al55wt%Cu. The alloys were processed in a 2000 kg capacity reverberatory furnace under a protective nitrogen gas atmosphere to prevent hydrogen and oxygen contamination. No grain refiners were added to the melt. The ingots used were pre-modified with strontium. Cast chilled wedges were re-melted at the University of Windsor using 1.5kg capacity, ceramic, bottom-drained crucibles. Simulating the Cosworth process, these twelve melts were held for 12 hours in the Lindberg™ resistance furnace set at $740°C^{+/-5}$ and continuously supplied with protective argon gas. Before each casting of an AlTAP test sample, the melt surface was carefully skimmed and the melt was thoroughly mixed to ensure homogeneous composition of all cast samples.

Test samples with average mass $300\ g^{+/-10}$ were poured into specially manufactured, ultra-light cups made out of 0.025 mm thick SS304 stainless steel foil (mass = $2.5\ g^{+/-0.2}$) maintaining the standard dimensions D = 50 mm, H = 60 mm. The temperatures were measured using specially designed, supersensitive Omega™ K type thermocouples, d = 0.12 mm wires sheathed with a 1.68 mm dual-channel ceramic straw. Only the welded tip coated with colloidal graphite film was directly exposed to the melt.

The total mass of the cup and the immersed thermocouple were less than 1% of the tested sample mass which is negligible as far as the thermal mass is concerned. These conditions, together the simultaneously calibrated thermocouples, the data acquisition system as well as the non-turbulent filling of the test cup help to guarantee that the recorded AlTAP signals represented, as closely as practically possible, the cooling and solidification processes of the tested alloy only. Resulting unbiased thermal data was collected using a high-speed National Instruments Data Acquisition System linked to the AlTAP computer. Each alloy trial was repeated three times.

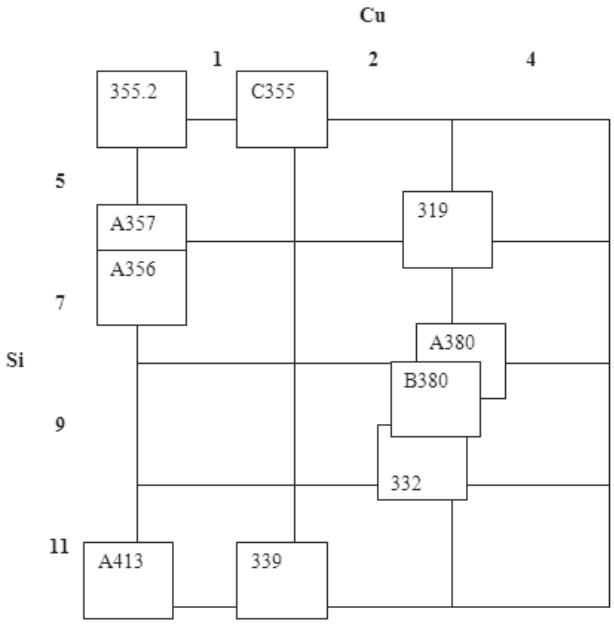

Fig. 20. Matrix of Si and Cu Nominal Compositions (wt.%) used in experiments with overlaid compositions of selected 3XX alloys

4.4. Results

Figures 21-23 provide easy visual interpretations for the resulting f_s vs. temperature of the analyzed alloys (only one trial per chemical composition is shown). The plots are grouped by the constant nominal 1, 2 and 4 wt.% Cu levels and variable Si levels.

By analyzing all recorded fraction solid curves (such as the ones in Figures 21-23) for all the trials in the experiments, a complete catalogue of temperature and f_s data was assembled. The average value for each of the three trials was taken. All standard deviations for the averages were found to be in the range 0.0 to 6.2°C (avg. standard deviation was 1.1). This data was then plotted in Matlab in order to create the graphs shown in Figures 24-41 which relate the chemistries to temperature and f_s.

Close inspection of Figures 24-41 revealed:

1. The liquidus temperature decreases considerably (a range of 64.9°C) with the increase of Si_{EQ} and Cu concentration, but solidus temperatures remain practically unchanged (a narrow range of 477.1-484.8°C). This has an effect on the solidification range (T_{liq} - T_{sol}), which declines from 142.1 to 89.6°C, with an increasing concentration of solutes (Si_{EQ} and Cu).
2. For the given Cu and Si_{EQ} levels, the range of the nucleation temperature of AlSi eutectic is narrow and does not exceed 22.3°C. $T^{AlSi}_{E\ NUC}$ also has a tendency to decrease with an increase in Cu levels (Figure 31).

Table 3.
Chemical Composition (analyzed by using Optical Emission Spectroscopy) and calculated Si_{EQ} of 12 Experimental Alloys (wt,%). Nominal Composition Si/Cu is used as an Alloy Label
(Note: Si_{EQ} does not include Cu)

Alloy Label	Si	Cu	Fe	Mg	Mn	Zn	Ti	Sr	Al	Si_{EQ}^{*}
5/1	4.85	1.03	0.09	0.14	0.01	0.01	0.058	0.0009	Balance	4.875
5/2	5.01	2.06	0.10	0.15	0.01	0.01	0.062	0.0012	“	5.038
5/4	4.89	3.85	0.09	0.16	0.01	0.01	0.057	0.0035	“	4.918
7/1	7.13	0.96	0.12	0.28	0.00	0.01	0.098	0.0029	“	7.138
7/2	7.05	1.98	0.13	0.28	0.00	0.01	0.094	0.0027	“	7.061
7/4	6.75	4.38	0.12	0.29	0.00	0.01	0.091	0.0029	“	6.764
9/1	9.16	1.05	0.12	0.31	0.00	0.01	0.100	0.0042	“	9.181
9/2	9.02	2.44	0.12	0.31	0.00	0.01	0.096	0.0063	“	9.032
9/4	8.95	4.38	0.14	0.27	0.01	0.01	0.090	0.0035	“	8.986
11/1	10.84	0.94	0.11	0.19	0.01	0.01	0.062	0.0029	“	10.876
11/2	10.67	1.95	0.10	0.16	0.01	0.01	0.061	0.0014	“	10.700
11/4	10.55	4.36	0.13	0.17	0.01	0.01	0.056	0.0034	“	10.605

1 The AlSi eutectic events have the highest variation in f_s and strongly depend on the alloy composition. In the case of $f_s^{AlSi_{EG}}$ (Figure 36), it decreases from 66.2% (5 $\mathbf{Si_{EQ}}$ / 1 Cu) to 17.7% for (11 $\mathbf{Si_{EQ}}$ /4 Cu).
2 The level of undercooling (maximums of 4.1°C for $T^{\alpha,DEN}{}_{UNDER}$ and 3.3°C for $T^{AlSi}{}_{UNDER}$) remains relatively small throughout the experiments and is not well correlated to changes in chemistry.
3 There is a relatively linear decrease in the variability of the metallurgical reaction temperatures going from the liquidus to the solidus temperatures.
4 In certain cases, such as $f_s^{\alpha,DEN}{}_{MIN}$ in Figure 26 and $f_s^{AlSi}{}_{UNDER}$ in Figure 38, maximums appear at low copper and intermediate levels of silicon as opposed to generally increasing or decreasing trends.

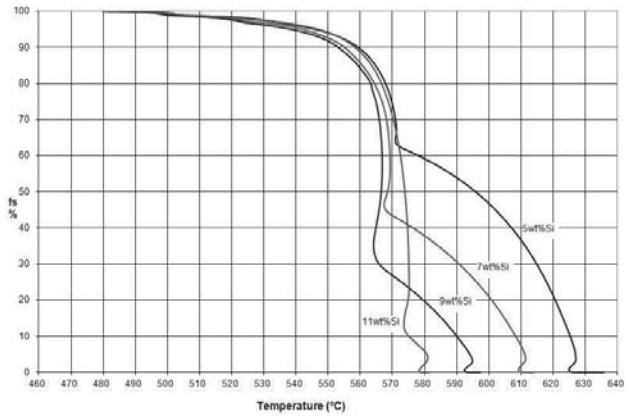

Fig. 21 - Fraction Solid Temperature Dependence for Nominal 1wt.% Cu and Nominal 5, 7, 9 and 11 wt.% Si

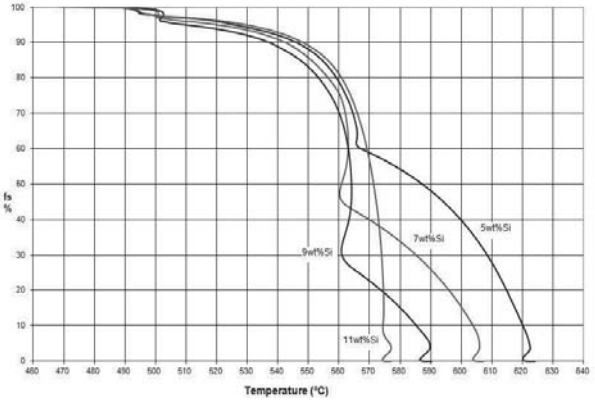

Fig. 22. Fraction Solid Temperature Dependence for Nominal 2wt.% Cu and Nominal Si 5, 7, 9 and 11 wt.% Si

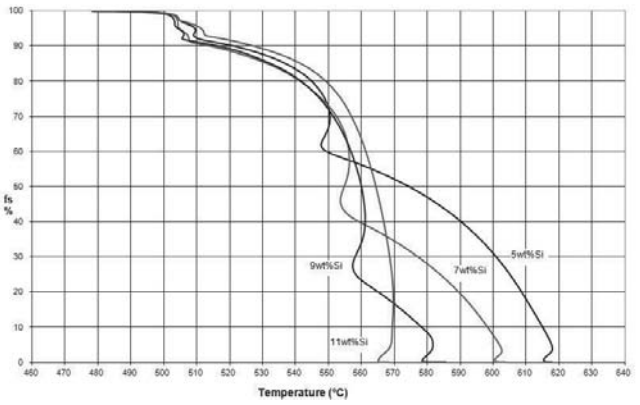

Fig. 23. Fraction Solid Temperature Dependence for Nominal 4.wt.% Cu and Nominal 5, 7, 9 and 11 wt.% Si

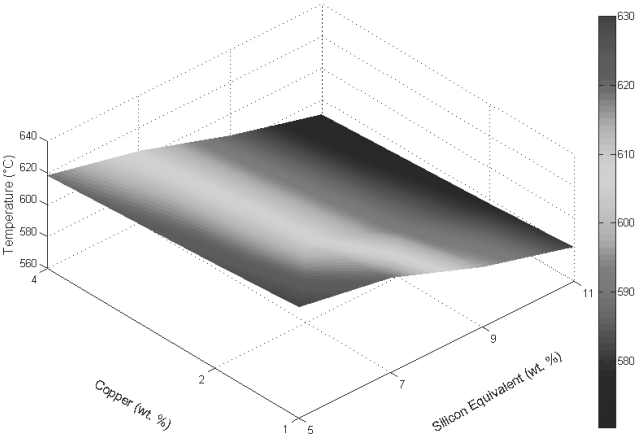

Fig. 24. $T^{\alpha,DEN}{}_{NUC}$ - Nucleation Temperature of αAl Dendrite Network (°C) vs. Cu (wt.%) and $\mathbf{Si_{EQ}}$ (wt.%)

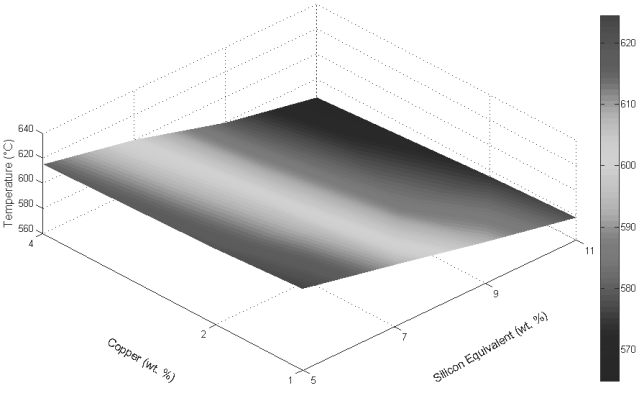

Fig. 25. $T^{\alpha,DEN}{}_{MIN}$ - Temperature of αAl Dendrite Network Minimum (°C) vs. Cu (wt.%) and $\mathbf{Si_{EQ}}$ (wt.%)

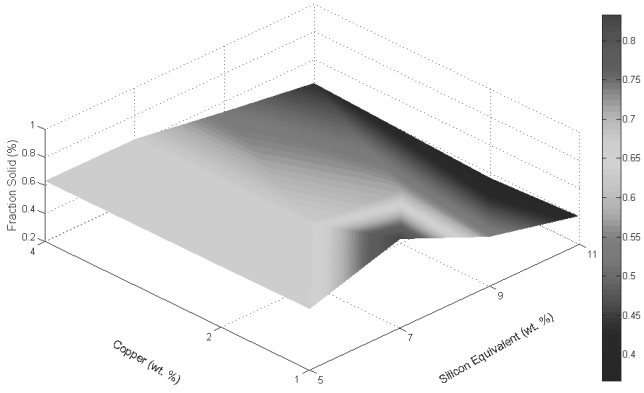

Fig. 26. $f_s^{\alpha,DEN}{}_{MIN}$ - Fraction Solid at αAl Dendrite Network Minimum Temperature (%) vs. Cu (wt. %) and **Si_{EQ}** (wt.%)

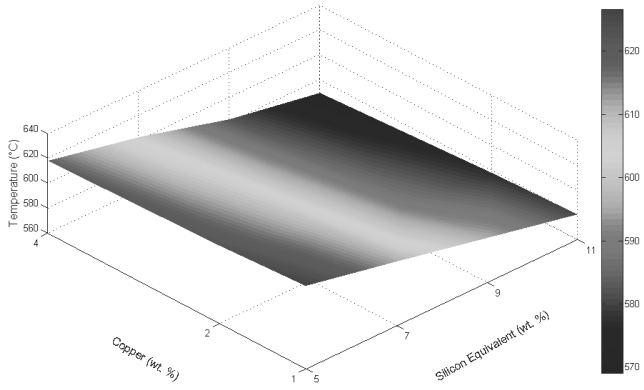

Fig. 27. $T^{\alpha,DEN}{}_{G}$ - Temperature of αAl Dendrite Network Growth (°C) vs. Cu (wt.%) and **Si_{EQ}** (wt.%)

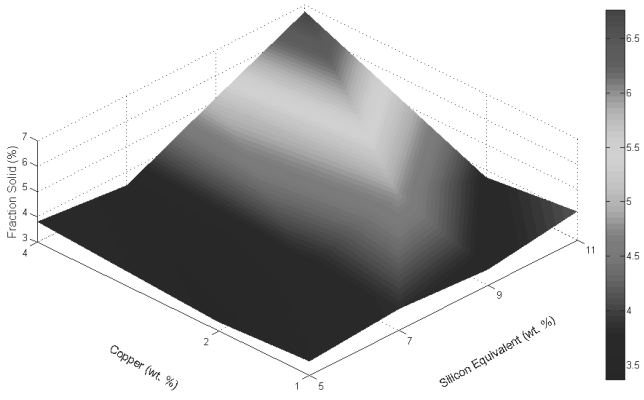

Fig. 28. $f_s^{\alpha,DEN}{}_{G}$ - Fraction Solid at αAl Dendrite Network Growth Temperature (%) vs. Cu (wt.%) and **Si_{EQ}** (wt.%)

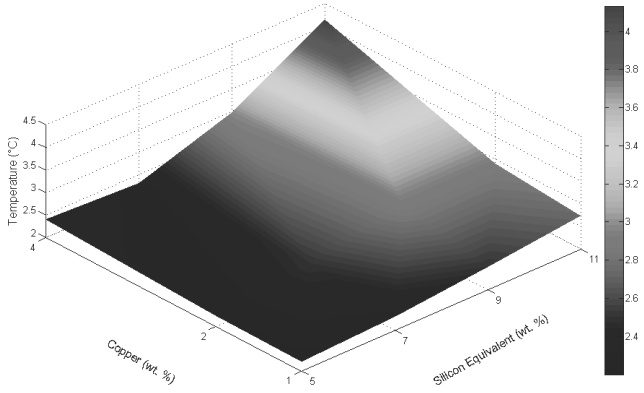

Fig. 29. $T^{\alpha,DEN}{}_{UNDER}$ - αAl Dendrite Network Undercooling (°C) vs. Cu (wt.%) and **Si_{EQ}** (wt.%)

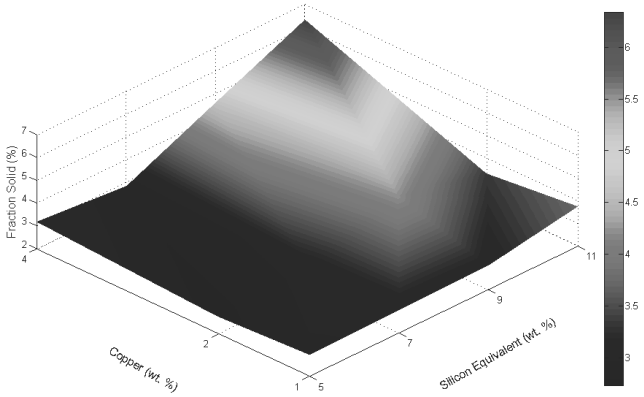

Fig. 30. $f_s^{\alpha,DEN}{}_{UNDER}$ - Fraction Solid Difference of αAl Dendrite Network Undercooling (%) vs. Cu (wt.%) and **Si_{EQ}** (wt.%)

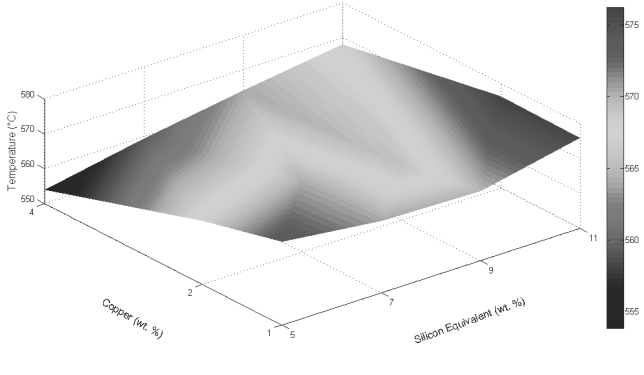

Fig. 31. $T^{AlSi}{}_{E\ NUC}$ - Temperature of AlSi Eutectic Nucleation (°C) vs. Cu (wt.%) and **Si_{EQ}** (wt.%)

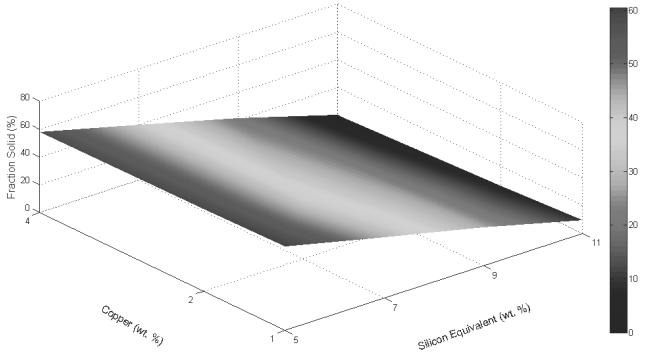

Fig. 32. $f_s^{AlSi}{}_{E\ NUC}$ - Fraction Solid at AlSi Eutectic Nucleation Temperature (%) vs. Cu (wt.%) and $\mathbf{Si_{EQ}}$ (wt.%)

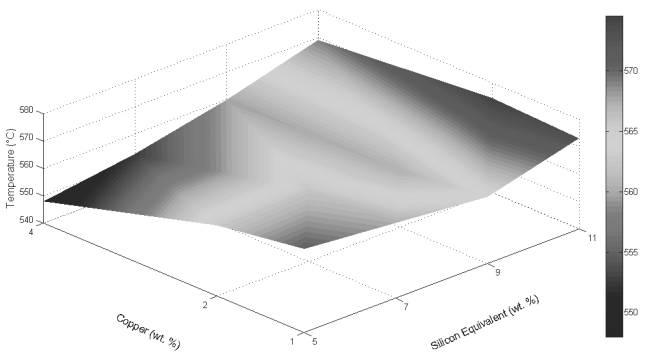

Fig. 33. $T^{AlSi}{}_{E\ MIN}$ - Temperature of AlSi Eutectic Minimum (°C) vs. Cu (wt.%) and $\mathbf{Si_{EQ}}$ (wt.%)

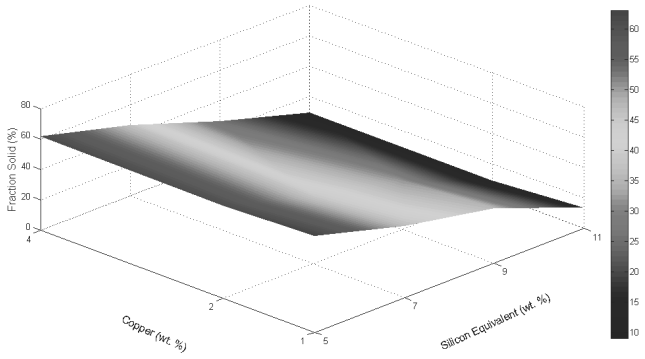

Fig. 34. $f_s^{AlSi}{}_{E\ MIN}$ - Fraction Solid at AlSi Eutectic Minimum Temperature (%) vs. Cu (wt.%) and $\mathbf{Si_{EQ}}$ (wt.%)

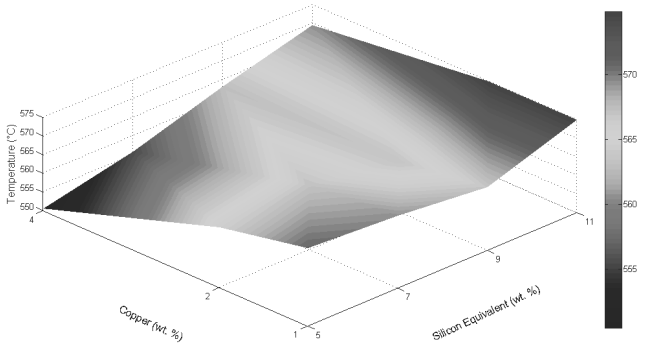

Fig. 35. $T^{AlSi}{}_{E\ G}$ - Temperature of AlSi Eutectic Growth (°C) vs. Cu (wt.%) and $\mathbf{Si_{EQ}}$ (wt.%)

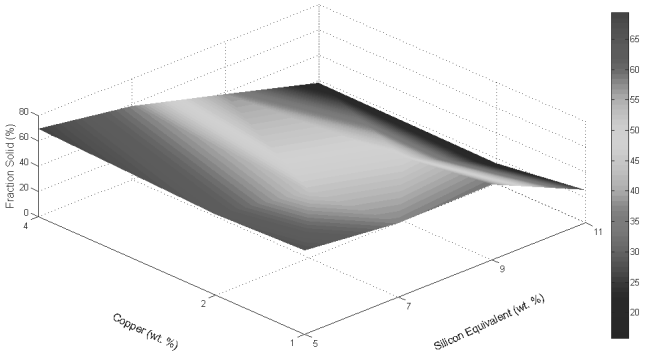

Fig. 36. $f_s^{AlSi}{}_{E\ G}$ - Fraction Solid at AlSi Eutectic Growth Temperature (%) vs. Cu (wt. %) and $\mathbf{Si_{EQ}}$ (wt.%)

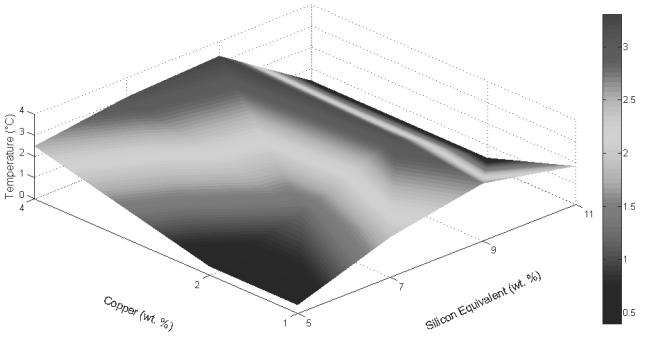

Fig. 37. $T^{AlSi}{}_{UNDER}$ - AlSi Eutectic Undercooling (°C) vs. Cu (wt. %) and $\mathbf{Si_{EQ}}$ (wt.%)

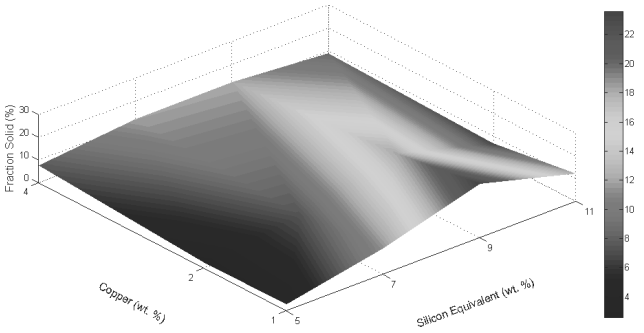

Fig. 38. $f_s^{AlSi}{}_{UNDER}$ - Fraction Solid Difference of AlSi Eutectic Undercooling (%) vs. Cu (wt.%) and **Si_{EQ}** (wt.%)

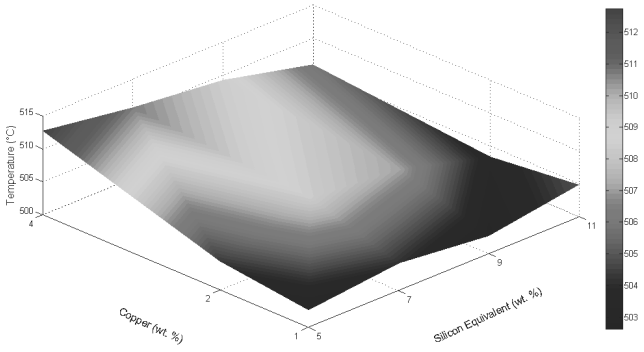

Fig. 39. $T^{AlSiCuMg}$ - Temperature of AlSiCuMg Eutectic (°C) vs. Cu (wt.%) and **Si_{EQ}** (wt.%)

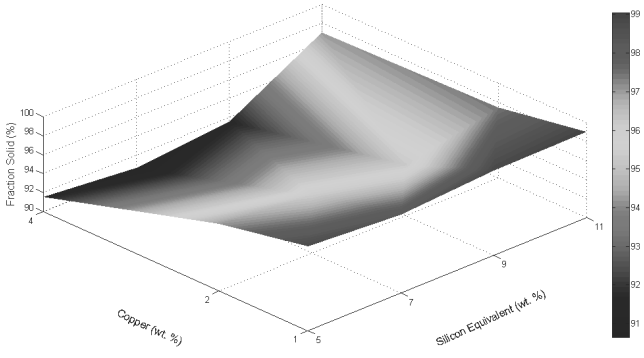

Fig. 40. $f_s^{AlSiCuMg}$ - Fraction Solid at AlSiCuMg Eutectic Temperature (%) vs. Cu (wt. %) and **Si_{EQ}** (wt. %)

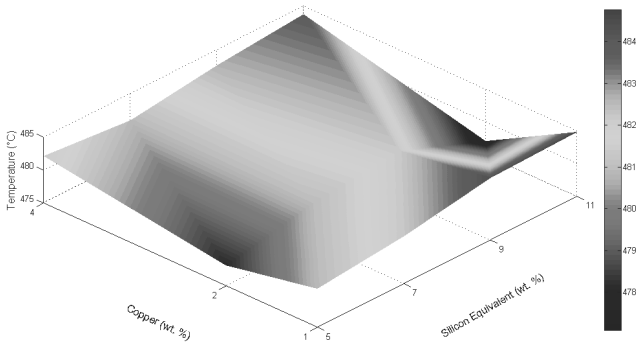

Fig. 41. T_{sol} - Solidus Temperature (°C) vs. Cu (wt.%) and **Si_{EQ}** (wt.%)

In order to better evaluate the strength of the trends seen in the graphs shown in Figures 24-41, the data was subjected to linear and polynomial plane fitting to find the planes of best fit. The correlation coefficient(s) (R^2) values from these fits are shown in Table 4. Though there are some excellent linear fits, especially for temperatures closer to the start of the cooling cycle, much of the data fits very well to 2nd degree planes, with 15 of the 18 values having an $R^2 > 0.80$.

Table 4.
Summary of correlation coefficients (R^2) for best fit planes

Symbol	Linear (1st degree)	Polynomial (2nd degree)
$T^{\alpha,DEN}{}_{NUC}$	0.990	0.993
$T^{\alpha,DEN}{}_{MIN}$	0.994	0.996
$f_s{}^{\alpha,DEN}{}_{MIN}$	0.618	0.842
$T^{\alpha,DEN}{}_{G}$	0.994	0.996
$f_s{}^{\alpha,DEN}{}_{G}$	0.554	0.778
$T^{\alpha,DEN}{}_{UNDER}$	0.708	0.890
$f_s{}^{\alpha,DEN}{}_{UNDER}$	0.600	0.814
$T^{AlSi}{}_{E\ NUC}$	0.787	0.933
$f_s{}^{AlSi}{}_{E\ NUC}$	0.997	0.999
$T^{AlSi}{}_{E\ MIN}$	0.638	0.926
$f_s{}^{AlSi}{}_{E\ MIN}$	0.986	0.994
$T^{AlSi}{}_{E\ G}$	0.723	0.932
$f_s{}^{AlSi}{}_{E\ G}$	0.834	0.944
$T^{AlSi}{}_{UNDER}$	0.080	0.851
$f_s{}^{AlSi}{}_{UNDER}$	0.205	0.751
$T^{AlSiCuMg}$	0.687	0.894
$f_s{}^{AlSiCuMg}$	0.781	0.940
T_{sol}	0.099	0.634

5. Summary and conclusions

A comparison of the results presented by various researchers who have calculated fraction solid dependence on temperature is a difficult task. This is due to the fact that the results depend on alloy composition, experimental conditions, the geometries of the systems, the instruments used and the sample cooling/solidification rates. In addition, alloy composition is frequently left unspecified, which complicates the comparative analysis. Therefore, only approximate comparisons can be made. For instance, compare the relationship between fraction solid and temperature derived from a series of experiments done for this paper with those taken from [25] (see Figure 14). Both sets of experiments used near pure aluminum (ingot purity was 99.95%). Nonetheless, differences are highly visible at the beginning and end of solidification. These differences may be due to the fact that the two sets of experiments were done at different cooling/solidification rates (approximately 1.6°C/sec for the present results and 3.0°C/sec in [25]) and likely the difference in the type and level of impurities present in these two ingots. Consequently, it is possible that in addition to the difference in the Al ingots purity level, the cooling/solidification rate also has an effect on its solidification characteristics.

This paper demonstrates that it is possible and justifiable to use a single and unique function for the "overall heat transmission coefficient" $\mathbf{U(T_c)}$. This function was used to describe the energy loss from solidifying test samples, for a given set of experimental conditions, over the temperature ranges measured in this study. AlTAP experiments on pure aluminum and aluminum 356 alloy yielded R^2 measurements close to 1.0, which suggests that the use of a single and unique function is a physically meaningful solution. The ***DBL*** derived from the actual $\boldsymbol{T_c}$ measurements is smooth and free of any discontinuities and represents the actually tested material and/or section of the cast component and its processing parameters. The ***DBL*** function is utilized in the AlTAP and UMSA Technology Platform software routines. These results made it possible to develop a method of calculating fraction solid based exclusively on the recorded solidification temperature in the centre of a test sample while its shape is not limited to a solid cylinder. This holds true for any metal, alloy and metallic composite tested regardless of its chemical composition, processing parameters and physical properties (aluminum, copper and iron alloys are the most commonly used). The only information that needs to be obtained from an experiment done under any conditions is the temperature $\mathbf{T_c}$ and its calculated first time derivative, $\mathbf{dT_c / dt}$. The data from these experiments was commercialized for the development of new high performance automotive cast components.

The results generated from the experiments on variable Si/Cu content showed that there are quantifiable trends in the fraction solid evolution and that in most cases they have a high correlation coefficient. The fraction solid information generated is not only applicable to current commercial alloys, but could also serve as a reasonable predictive model for fraction solid evolution of AlSi alloys beyond the chemistries investigated.

Acknowledgements

This research was funded by a Discovery Grant from the Natural Sciences and Engineering Research Council of Canada (NSERC) as well as AUTO21, a member of the Networks of Centres of Excellence of Canada program. The authors would like to acknowledge the assistance of the Nemak of Canada Corporation, Dr. M. B. Djurdjevic and Ms. E. Moosberger in the preparation of this paper.

References

[1] M.B. Djurdjevic, W. Kasprzak, C.A. Kierkus, J.H. Sokolowski, Quantification of Cu enriched phases in synthetic 3XX aluminum alloys using the thermal analysis technique, AFS Transactions, 2001.
[2] M. Djurdjevic, P. Gallo, H. Jiang, J.H. Sokolowski, Evaluation of strontium fading in the 319 aluminum alloy using thermal analysis, AFS Transactions 20 (2000) 485-486.
[3] M. Djurdjevic, T. Stockwell and J. H. Sokolowski, The effect of strontium on the microstructure of aluminum-silicon and aluminum-copper eutectics in the 319 Alloy, International Journal of Cast Metals Research 12 (1999) 67-73.
[4] M. Djurdjevic, W.T. Kierkus, R. Liliak, J.H. Sokolowski, Extended analysis of cooling curves, Proceedings of the 41st Conference of Metallurgists COM'2002, Montreal, 2002.
[5] H. Jiang, W. Kierkus and J. H. Sokolowski, Dendrite coherency point determination using thermal analysis and rheological measurements, Proceedings of the International Conference on Thermophysical Properties of Materials TPPM'99, Singapore, 1999.
[6] R. MacKay, M. Djurdjevic, J.H. Sokolowski, W. Evans, Using the method of a in-situ thermal analysis array in a cast section to assess riser feeding efficiency, Proceedings of the 131st TMS Annual Meeting, Seattle, Washington, 2002, 17-21.
[7] R. MacKay, M. Djurdjevic, et al., Effect of cooling rate on fraction solid of metallurgical reactions in 319 alloy, AFS Transactions 25 (2000) 521-529.
[8] X. Chen, W. Kasprzak, J.H. Sokolowski, Reduction of the heat treatment process for the Al-based alloys by utilization of heat from solidification process, Journal of Materials Processing Technology 176 (2006) 24-31.
[9] L. Bäckerud, G. Chai, J. Tamminen, Solidification characteristics of aluminum alloys, AFS-Skanaluminium, 1990.
[10] R. Mackay, J. Sokolowski, Experimental observations of dendrite coarsening and Al-Si eutectic growth in progressively quenched structures of Al-Si-Cu casting alloys, International Journal of Metalcasting Spring (2008) 57-80.
[11] J. Barlow, D.M. Stefanescu, Computer aided cooling curve analysis revisited, unpublished, 1996.

[12] W.T. Kierkus, J.H. Sokolowski, Recent advances in cooling curve analysis: A new method of determining the 'Base Line' equation, AFS Transactions 66 (1999) 161-167.
[13] E. Fras, W. Kapturkiewicz, A. Burbielko, H.F. Lopez, A New concept in thermal analysis of castings, AFS Transactions 101 (1993) 505-511.
[14] D. Emadi, L. Whiting, M. Djurdjevic, W.T. Kierkus, J.H. Sokolowski, Comparison of newtonian and fourier thermal analysis techniques for calculation of latent heat and solid fraction of aluminum alloys, Metalurgija (2004) 91-106.
[15] D.M. Stefanescu, G. Upadhya, D. Bandyopadhyay, Heat transfer-solidification kinetics modeling of solidifcation of castings, Metallurgical Transactions A 21 (1990) 997-1005.
[16] D.M. Stefanescu, Solidification of flake, compacted, vernicular and spheroidal graphite cast irons as revealed by thermal analysis and directional solidification experiments, Material Research Society Symposium Proceedings, 34, 1985.
[17] K.G. Upadhya, D.M. Stefanescu, K. Lieu, D.P. Yaeger, Computer-aided cooling curve analysis: principles and applications in metal casting, AFS Transactions 97 (1989) 61-66.
[18] S.H. Jong, W.S. Hwang, Study of functional relationships of fraction solid with temperature in mushy range for the A356 Al alloy, AFS Transactions 92 (1992) 939-946.
[19] J. Tamminen, Thermal analysis for investigation of solidification mechanisms in metals and alloys, Chemical Communications, University of Stockholm, 1988.
[20] L. Arnberg, L. Bäckerud, Solidification characteristics of aluminum alloys, Vol. 3: Dendrite coherency, American Foundrymen's Society, Inc, 1996.
[21] H. Jiang, W.T. Kierkus, J.H. Sokolowski, Determining dendrite coherency point characteristics of Al alloys using single-thermocouple technique, AFS Transactions 68 (1999) 169-172.
[22] R. Chavez-Zamarripa, J. Angelica Ramos-Salas, J. Talamentes-Silva, S. Valtierra, R. Colas, Determination of the dendrite coherency point during solidification by means of thermal diffusivity, Metallurgical and Materials Transactions A 38 (2007) 1875-1879
[23] S. Gowri, Comparison of thermal analysis parameters of 356 and 359 alloys, AFS Transactions 94-29 (1994) 503-508.
[24] H.G. Kang, H. Miyahara, K. Ogi, Influence of cooling rate and additions of Sr and Ti-B on solidification structures of AC4B type alloy, Proceedings of the 3rd Asian Foundry Congress, edited by Z.H. Lee, C.P. Hong, M.H. Kim, The Korean Foundrymen's Society, Kyongju, Korea, 1995, 108-115.
[25] Y.F. Chen, S.H. Jong, W.S. Hwang, The effect of cooling rate on the latent heat released mode for near pure aluminum and aluminum silicon alloy, Modelling of casting, welding and advanced solidification processes VII Edition by M. Cross, J. Campbell, The Minerals, Metals and Materials Society (1995) 483-490.
[26] L. Ananthanarayanan, F.H. Samuel, J. Gruzleski, The thermal analysis studies on the effect of cooling rate on the microstructure of the 319 aluminum alloy, AFS Transactions 92-141, 383-391.
[27] A.M. Figueredo, Y. Sumartha, M.C. Flemings, Measurement and calculation of solid fraction in quenched semi-solid melts of rheocast aluminum alloy A357, Light Metals edited by Barry Welch, The Minerals, Metals and Materials Society, 1998, 1103-1106.
[28] G. Chai, Dendrite coherency during equiaxed solidification in aluminum alloys, Ph.D. Thesis, Department of Structural Chemistry, Arrhenius Laboratory, Stockholm University, 1994.
[29] L. Arnberg, L. Bäckerud, G. Chai, Solidification characteristics of aluminum alloys, Vol. 3: Dendrite Coherency, American Foundrymen's Society, Inc., Des Plaines,1996.
[30] E. Tzimas, A. Zavaliangos, Evaluation of volume fraction of solid in alloys formed by semisolid processing", Journal of Materials Science 35 (2000) 5319-5329.
[31] J. Wannasin, R. Canyook, R. Burapa, L. Sikong, M.C. Flemings, Evaluation of solid fraction in a rheocast aluminum die casting alloy by a rapid quenching method, Scripta Materialia 59 (2008) 1091-1094.
[32] M.C. Flemings, Solidification processing, McGraw-Hill, Inc., 1972.
[33]S. Ohta, K. Asai, The behaviour of temperature decreasing and fraction solid increasing in solid-liquid coexisting zone in solidification process of aluminum alloy weld metal, Transactions of the Japan Welding Society 24/2 (1993) 131-139.
[34] N. Saunders, Phase diagram calculations for commercial Al-alloys, Material Science Forum SF2M and INPG, Grenoble, 217-222/2 (1996) 667-672.
[35] J.H. Chen, H.L. Tsai, Comparison of different models of latent heat release for modeling casting solidification, AFS Transactions (1990) 539-546.
[36] C.S. Kantekar, D.M. Stefanescu, Macro-micro modeling of solidification of hypoeutectic and eutectic Al-Si alloys, AFS Transactions 60 (1988) 591-598.
[37] H. Huang, V.K. Suri, J.L. Hill, J.T. Berry, Heat source/sink algorithm for modeling phase changes durings in castings and water evaporation in green sand molds, AFS Transactions) 54 (1991) 685-689.
[38] M. Rapaz, Modeling of microstructure formation in solidification processes, International Materials Reviews 34/3(1989) 93-123.
[39] W. Kurz, D.J. Fisher, Fundamentals of solidification, Trans Tech Publications, U.K.-USA, 1986.
[40] S. Jeng, S. Chai, Determination of the solidification characteristics of the A356.2 aluminum alloy, Material Science Forum 217-222 (1996) 283-288.
[41] M. Kiuchi, S. Sigiyama, A new method to detect solid fraction of mushy/semi solid metals and alloys, Annals of the CIRP 43/1 (1994) 271-274.
[42] N. Saunders, Z. Guo, A.P. Miodownik, J.-Ph. Schillé, Modelling the material properties and behaviour of Ni- and NiFe-based superalloys, Superalloys 718, 625, 706 and Various Derivatives (2006) 571-580.
[43] K.P. Sołek, R.M. Kuziak, M. Karbowniczek, The application of thermodynamic calculations for the semi-solid processing design, Archives of Metallurgy and Materials 52/1 (2007) 25-32.

[44] M.B. Djurdjevic, W.T. Kierkus, et al., Modeling of fraction solid for the 319 aluminum alloy, AFS Transactions 14 (1999) 173-179.
[45]A. Zavaliangos, E. Tzimas, On the approximation of the partial areas method in the calculation of the fraction of solid, Metallurgical and Materials Transactions B-Process Metallurgy and Materials Processing Science 31/4 (2000) 877-879.
[46] M.B. Djurdjevic, A. Mitrasonovic, J.H. Sokolowski, Development of the Silicon Equivalent (SiEQ) algorithm and its application for calculation of the characteristic temperatures of solidification multi-component 3XX series of Al alloys, Proceedings of the 15th International Conference and Exposition for the Foundry Industry, Monterrey, Mexico, 2003, 214-226.
[47] F.C.R. Hernandez, M.B. Djurdjevic, W.T. Kierkus, J.H. Sokolowski, Calculation of the liquidus temperature for hypo and hypereutectic aluminum silicon alloys, Materials Science and Engineering A 396/1-2 (2005) 271-276.
[48] J.L. Murray, A.J. McAlister, The Al-Si (aluminum-silicon) casting system, Bulletin of Alloy Phase Diagrams 5/1 (1984) 74-84.
[49] W.J. Boettinger, U.R. Kattner, K.W. Moon, J.H. Perepezko, DTA and heat-flux DSC measurements of alloy melting and freezing, NIST Recommended Practice Guide Special Publication 960-15, National Institute of Standards and Technology,Washington, DC, 2006.